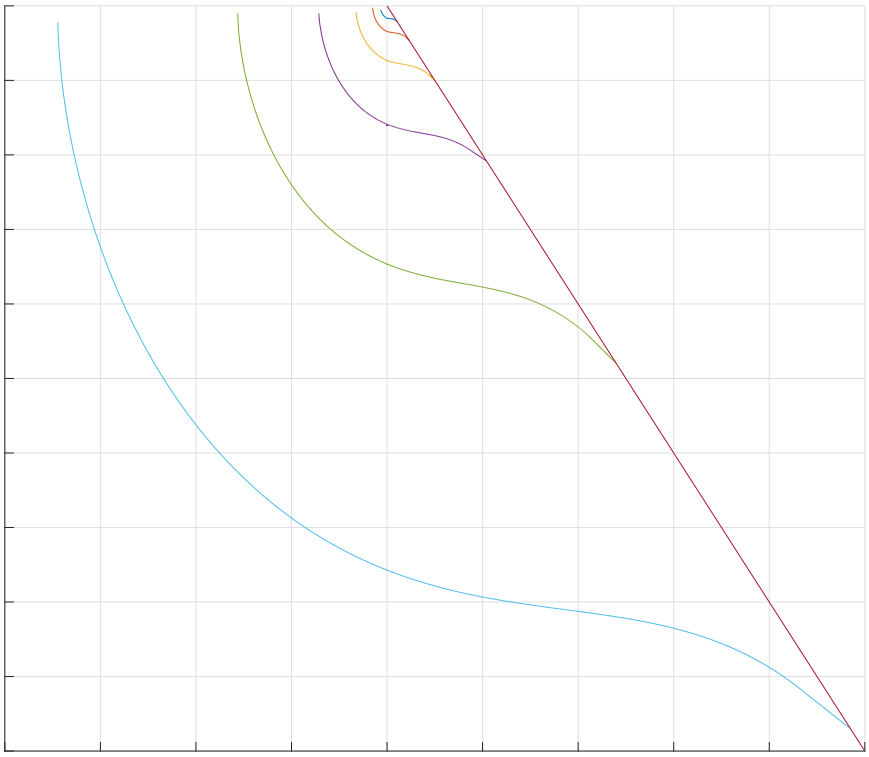

Zero-Range Three-Body Physics in Ultracold Bosonic Gases

Master's thesis in Physics

KIRILL DANILOV

DEPARTMENT OF PHYSICS
CHALMERS UNIVERSITY OF TECHNOLOGY
Gothenburg, Sweden 2022
www.chalmers.se

Master's thesis 2022

Zero-Range Three-Body Physics in Ultracold Bosonic Gases

KIRILL DANILOV

CHALMERS
UNIVERSITY OF TECHNOLOGY

Department of Physics
Chalmers University of Technology
Gothenburg, Sweden 2022

Zero-Range Three-Body Physics in Ultracold Bosonic Gases
KIRILL DANILOV

Supervisor: Johannes Hoffmann, University of Gothenburg, Department of Physics
Examiner: Henrik Johannesson, University of Gothenburg, Department of Physics

Master's Thesis 2022
Department of Physics
Chalmers University of Technology
SE-412 96 Gothenburg
Telephone +46 31 772 1000

Cover: Three body state binding energy spectrum for identical bosons.

Typeset in LaTeX
Printed by Chalmers Reproservice
Gothenburg, Sweden 2022

Zero-Range Three-Body Physics in Ultracold Bosonic Gases
Kirill Danilov
Department of Physics
Chalmers University of Technology

Abstract

Due to their universality, effective field theories developed in the study of nuclear physics have found a direct application in the research of many-body physics in quantum degenerate gases such as Bose-Einstein condensates. This thesis will reproduce from one such theory, the zero-range model, the discrete scaling symmetries emergent for the physical observables of three-body physics in bosonic gases within the ultracold temperature regime. The conditions of the ultracold regime allow for the treatment of bosonic gas atoms as quantum-mechanical point particles interacting exclusively through scattering in the s-wave channel. The Feynman rules of the zero-range model are derived and implemented to formulate the three-body scattering amplitude and the three-body bound state equation using the inclusion of an auxiliary diatomic field operator.
The zero-range model has been shown to be renormalisable within the three-body sector utilizing a renormalisation group limit cycle through numerical tests of an ultraviolet cutoff momentum dependent three-body scaling term $G(\Lambda)$ parametrised by a three-body parameter Λ_*. The universal properties of the Efimov effect have been confirmed for the three-body physics of a single species of bosonic gas, as well as for mixtures of species distinguished by different masses. Furthermore, results for the three-body scattering amplitude demonstrate the impact of different parameters Λ_* and two-body scattering lengths on the three-body scattering length of the quantum degenerate gas.
In conclusion, the zero-range model enables the description of few-body physics of bosonic quantum degenerate gases with respect to a finite set of parameters: the masses of gas species, the spin-statistic of gas species, the two-body scattering length and the three-body parameter, and the temperature of the gas.

Keywords: Bose-Einstein gas, Efimov effect, ultracold, universality, zero-range model.

Acknowledgements

I would like to acknowledge my supervisor, Professor Johannes Hofmann, for his lengthly and thorough coordination of my work, and my family for their invaluable support to the fulfillment of my education.

Kirill Danilov, Gothenburg, December 2021

Nomenclature

Below is the nomenclature of indices, constants, parameters, variables, operators and Feynman diagrams that have been used throughout this thesis.

Indices

i, j, n, n', N	Generic indices
l	Quantum mechanical angular momentum number
s, I	Quantum mechanical spin, nuclear spin state number
f, i	Final and initial states

Constants

k_B	Boltzmann's constant
$\hbar$	Reduced Planck's constant
λ_0	Bare two-body coupling constant
Z_Ψ	Dimer field renormalisation constant
γ_0	Bare three-body coupling constant

Parameters

m, m_r	Mass, reduced mass
T	Gas temperature
λ_T	Thermal de Broglie wavelength
n	Gas particle density
l_vdW, r_s	Van der Waals length, effective range
a, a_2, a_AD	Two-body scattering length, bare two-body scattering length, atom-dimer scattering length

Λ_*, κ_*	Three-body parameter
λ	Discrete scaling symmetry parameter
r_m	Mass ratio
Λ	Ultraviolet cutoff momentum

Variables

k, q_i, p_i	Wavevector, momentum of quantum-mechanical point particle i
$\omega, \omega_T, E_{\text{type}}$	Frequency, energy of channel T, generic energy by context
δ_l	Phase shift at angular momentum number l
$\boldsymbol{r}_i$	Position of QM particle i
t_i	Time of QM particle i
$\psi_{\text{scatter}}, \lvert\psi^+\rangle$	Scattering wavefunction, outgoing scattering wavefunction state
f_l, A_l	Partial wave amplitude, radial scattering wavefunction
C	Modified three-body scattering amplitude function
$G(\Lambda)$	Three-body scaling term at ultraviolet cutoff Λ

Operators

H, $\mathcal{H}$	Hamiltonian, Hamiltonian density
V	Interaction potential
$U(t, t_0)$	Quantum-mechanical unitary time-evolution operator
$\mathcal{S}, \mathcal{T}$	Matrices for quantum-mechanical state evolution
$\psi, \psi^\dagger$	Atomic field annihilation/creation operators
$\Psi, \Psi^\dagger$	Dimer field annihilation/creation operators
$T\{\}$	Time-ordering operator

Feynman Diagrams

$\mathcal{F}^N_{\text{fields}}$	Generic Feynman diagram at N loop level, the field operators involved listed in subscript
$\mathcal{A}_n$, $\mathcal{A}_{n,l=0}$, $\mathcal{A}^+$	n-body scattering amplitude, n-body scattering amplitude projected on total angular momentum $l = 0$, high-momenta contributions to the scattering amplitude
D_{field}	Propagator for a quantum field operator

Contents

1

Introduction

In theoretical physics, it is typically challenging to formulate a detailed and accurate understanding of any complex system without applying some sensible intuition to the problem. Non-relativistic effective field theories, utilized frequently in the study of strongly-interacting particles such as the constituent subatomic particles of nuclei, resort to the separation of energy scales in a system in order to reduce the amount of unnecessary detail of the problem. Through understanding that the relevant phenomena for the desired observables at a given energy scale will not be affected by conditions that occur as a result of higher-energy interactions, it is possible to greatly simplify the theory modelling a physical interaction down to the dependence on a handful of manipulable or observable parameters, as long as the low-energy conditions are met.

A prediction made in 1971 by Vitaly Efimov stated that subatomic particles could, if their scattering was of sufficiently low kinetic energies, form weakly bound three-body states [1]. This prediction would start the development of effective field theories in order to understand the conditions under which these bound three-body states could form and what the recombination rates into other configurations would be [2]. Despite the steady progress of the mathematical science applied to these theories, in particular the introduction of renormalisation group transformations by Wilson [3], there was little fortune in providing the experimental results to confirm or reject Efimov's theories within the scope of nuclear physics itself.

In parallel to these developments, the science of ultra-cold states and materials made some of its most significant breakthroughs when the Bose-Einstein condensate was created for the first time in laboratory conditions in 1995, and when its half-integer counterpart, the degenerate Fermi gas was first contained in optical trapping in 2001 [4]. The study of these quantum degenerate gases utilized the possibility to trap ultracold with optical tweezer technology and to tune the strength of the two-body interactions between gas atoms with the use of magnetic fields, allowing experimentalists to create strongly interacting gases. Studies on degenerate quantum gases have included, for example, ^{40}K, ^{6}Li, ^{7}Li, ^{87}Rb and ^{23}Na [5], [6]. More recently Bose-Einstein condensates have also been realised for ^{39}K and metastable ^{4}He, and dipolar degenerate Fermi gas was realised from ^{167}Er [7], [8], [9]. Although different from nuclear particles, in 2005 quantum degenerate gas atoms were found to be a valid experimental proving ground for the study of many-body physics [10], and the predictions of Efimov physics due to the universal properties of the effective field theories that governed them both in the ultracold regime [11].

This thesis documents a work that aims to detail the effective field theories developed from nuclear physics and apply these in the study of strongly interacting quantum

degenerate gases in the ultracold temperature regime. In chapter 2, we cover the physical arguments that motivate the implementation of an effective field theory derived from nuclear physics as a model for quantum degenerate gases. In chapter 3 we will derive the effective field theory, known as the zero-range model, used in conjunction with numerical methods discussed in the appendix B.1 to demonstrate the physical observables of three-body physics that are then presented in chapter 4 along with a discussion of how these three-body observables may be reflected in the experimental studies of quantum degenerate gases. The thesis is closed by concluding remarks in chapter 5.

2

Background

In this chapter, we introduce the foundation for the effective field theories used for describing degenerate quantum gases in the ultra-cold regime. Section 2.1 covers the distinction between degenerate quantum gases and classical gases at ultracold temperatures, i.e. below 1 μK. Section 2.2 discusses the various scales of energy inherent to the interactions of atoms in a gas, defines the natural energy scale and establishes that in the degenerate limit the atoms can be treated as quantum mechanical point particles. Sections 2.3 and 2.4 discuss quantum-mechanical two-body scattering, introduce the s-wave scattering length and demonstrate that in the ultra-cold regime, scattering is dominated by the s-wave channel. Section 2.5 describes universal properties of degenerate quantum gases that are expected to arise as the result of the Efimov effect.

2.1 Degenerate Quantum Gases: Macroscopic Level

Atoms in the gas phase exhibit particular behaviour as the quantum-physical realm is reached. At high temperatures, dilute gases are modelled as point-like particles that follows the Maxwell-Boltzmann distribution, for particles with momentum $\boldsymbol{p}$,

$$f(\boldsymbol{p}) = \frac{1}{(2\pi m k_B T)^{\frac{3}{2}}} e^{-\frac{\boldsymbol{p}\cdot\boldsymbol{p}}{2mk_BT}}, \tag{2.1}$$

where m is the mass of the gas particles, k_B is Boltzmann's constant and T is the gas temperature. To procure the quantum-mechanical limit, we set the wavevector $k = \frac{\boldsymbol{p}}{2\pi\hbar}$ and renormalise equation 2.1:

$$(\frac{mk_BT}{2\pi\hbar^2})^{\frac{3}{2}} \int dk^3 e^{-\frac{4\pi^2\hbar^2 k\cdot k}{2mk_BT}} = 1$$

Reading off the forefactor gives a characteristic length scale, the thermal de Broglie wavelength:

$$\lambda_T = \sqrt{\frac{2\pi\hbar^2}{mk_BT}}. \tag{2.2}$$

The thermal de Broglie wavelength can be thought of as the average size of the atoms as quantum-mechanical wave packets. When it is comparable to the other length scales, such as the interparticle separation, it is not possible to disregard the emergent quantum physics. In order to make an estimate of the temperature at which the quantum effects become relevant, we make the following comparison

Temperature (K)	273	1	1×10^{-3}	1×10^{-6}
λ_T (μm)	1.1×10^{-5}	1.9×10^{-4}	5.9×10^{-3}	1.9×10^{-1}

Table 2.1: Thermal de Broglie wavelength at 300 K, 1 K, 1 mK and 1 μK. for ^{87}Rb, with mass $m = 1.44 \times 10^{-25}$ kg.

between the values for the wavelength λ_T of ^{87}Rb at temperatures ranging from temperature at 300 K to near absolute 0 at 10^{-1} K.
For any dilute gas the volume per particle exceeds the volume of tha gas, therefore the interatomic separation $n^{-\frac{1}{3}}$ is much greater than the radii of the atoms. An assessment of the interatomic separation of degenerate quantum gases can be made from the example of a ^{87}Rb Bose-Einstein condensate, which was observed to have density $n = 2.5 \times 10^{18}$ m^{-3} [12]. Therefore:

$$n^{-\frac{1}{3}} \approx 0.7 \times 10^{-6} \text{ m} = 0.7 \ \mu\text{m}. \tag{2.3}$$

Comparing with table (2.1), at $T = 300$ K the thermal de Broglie wavelength is much smaller than the interatomic separation, so there are no discernible quantum mechanical effects and atoms may be regarded as classical particles. If the temperature is lowered, the thermal de Broglie wavelength increases and quantum mechanical effects become significant to the statistical properties of the gas. At temperatures below $T = 10^{-6}$ K, the statistics of the atoms are not the classical Maxwell-Boltzmann distribution, but instead either the Bose-Einstein or the Fermi-Dirac distributions,

$$f_{\text{BE}}(E) = \frac{1}{e^{\frac{E}{k_B T}} - 1}, \qquad f_{\text{FD}}(E) = \frac{1}{e^{\frac{E}{k_B T}} + 1}.$$

The macroscopic properties of the degenerate quantum gas and the nature of its degenerate phases are depend on the Bose - or Fermi statistics of the atoms. The spin statistic is dependent on a particle's nuclear composition and electron number, where each fermion contributes $\frac{1}{2}$ spin. Bosonic isotopes will have full integer spin while fermionic isotopes will have half-integer spin.

2.2 Energy scales

The internal energies of atoms includes excitation energies of the electron into greater orbitals, the interaction between electron, the nuclear level splitting known as the hyperfine energy, and the magnetic-spin interaction of the electron in the presence of a magnetic field. For many-body systems, the relevant energies are the kinetic energy of the gas and the interaction energy between atoms, which consists of van der Waals forces and the short-range contact potentials.
To demonstrate the energy scale of electronic excitation, we use the alkali metals as an example. The first electronic excitation of alkali atoms scales as E_{Ryd}/N^2 where $E_{\text{Ryd}} = 13.6$ eV is the excitation of hydrogen. For the lowest value such as $\frac{13.6}{6^2}$ eV in the case of ^{133}Cs, the corresponding temperature scale is $T_{\text{elec}} \approx 10^3$ K.

The hyperfine splitting energy $E_I = \frac{2}{2I+1}E_{\rm hf}$ and magnetic energy $E_{\rm m} = \mu B = 2\mu_B B$ contribute to the internal energy of the atom due to the interaction of the nuclear spin , with quantum number I, with the electron spin s, and the interaction of the electron spin with any applied magnetic field. The temperature scales for experiments at a magnetic field of 2×10^{-2} T are $T_{\rm hf} \approx 10^{-1}$ K and $T_{\rm m} \approx 10^{-2}$ K [6]. The potential energy of the many-body system is determined by interactions of the gas atoms through short-range contact potentials $V_{\rm short}$ with long-range van der Waals tails. The van der Waals contribution is caused by the polarizability and motion of electron clouds in the atoms [13]. At distances larger than the radius of the atoms, the van der Waals long-range tail has the form $V_{\rm vdW}(r) \sim -\frac{C_6}{r^6}$.

$$V(r) = V_{\rm short}(r) - \frac{C_6}{r^6}. \tag{2.4}$$

The van der Waals length $l_{\rm vdW}$ follows from dimensional analysis, where $[E]$ is the dimension of energy and $[L]$ is the dimension of length:

$$[C_6] = [E][L]^6, \qquad [\frac{\hbar^2}{m}] = [E][L]^2, \qquad [\frac{mC_6}{\hbar^2}] = [L]^4,$$

Hence,

$$l_{\rm vdW} := (\frac{mC_6}{\hbar^2})^{\frac{1}{4}}. \tag{2.5}$$

The corresponding energy scale is

$$E_{\rm vdW} = \frac{\hbar^2}{ml_{\rm vdW}^2} = \frac{\hbar^3}{\sqrt{m^3C_6}}. \tag{2.6}$$

The van der Waals energy is the natural interaction energy scale of the system. Using results for ^{87}Rb atom [14]:

$$E_{\rm vdW}[^{87}{\rm Rb}] = 6.4\times10^{-9}\ {\rm eV}, \qquad l_{\rm vdW}[^{87}{\rm Rb}] = 8.6\times10^{-9}\ {\rm m}.$$

In terms of temperature, the scale is $T_{\rm vdW} \approx 10^{-4}$ K.
The particle density of the gas sets an additional characteristic scale, the Fermi energy $E_{\rm F}$. For transitioning to the ultra-cold phase necessary to obtain a degenerate quantum gas, the thermal energy $k_BT = \frac{2\pi^2\hbar^2}{m\lambda_T^2}$ must be similar to the Fermi energy, so that the thermal wavelength λ_T will exceed the interatomic separation of the atoms $n^{-\frac{1}{3}}$:

$$E_{\rm F} = \frac{\hbar^2(3\pi)^{\frac{2}{3}}n^{\frac{2}{3}}}{2m} \sim k_{\rm B}T. \tag{2.7}$$

In a condensate of ^{87}Rb the Fermi energy in terms of temperature is $T_{\rm F} \approx 10^{-8}$ K. The energy scales of the atomic structure ΔE_1, E_I and $E_{\rm m}$ exceed the energy scales of the many-body system $E_{\rm vdW}$ and $E_{\rm F}$. The various energy scales are summarised in table 2.2.
Experiments typically contain and manipulate the gas using lasers for optical trapping and cooling of the sample. As the first order approximation of the restoring force in optical trapping is linear, the potential of such optical wells is modelled as harmonic. If the gas is subject to confinement by optical trapping, the lowest scale

ΔE_1	First electronic excitation	E_{Ryd}/N^2	10^3 K
E_I	Hyperfine splitting	$\frac{2}{2I+1}E_{\mathrm{hf}}$	10^{-1} K
E_{m}	Magnetic energy	$B \sim 10^{-2}$ T, μB	10^{-2} K
E_{vdW}	van der Waals energy	$\frac{\hbar^3}{\sqrt{m^3 C_6}}$	10^{-4} K
E_{F}	Fermi energy	$\frac{\hbar^2 (3\pi)^{\frac{2}{3}} n^{\frac{2}{3}}}{2m}$	10^{-8} K
E_{well}	Confining optical well	$\hbar\omega_{\mathrm{well}}$	10^{-10} K

Table 2.2: Energy scales relevant to a quantum gas in descending order.

of energy are the energy differences of the harmonic potential. The energy levels of a harmonic potential are spaced as $\hbar\omega_{\mathrm{well}}$ where a typical frequency is $\omega_{\mathrm{well}} = 2\pi 10$ Hz [6]. The corresponding temperature scale is $T_{\mathrm{well}} \approx 10^{-10}$ K.
When the gas is at a temperature where $k_{\mathrm{B}}T$ is comparable or below E_{vdW}, any atomic interactions will be unable to cause state transitions of the atoms between spin, hyperfine or electronic levels. At even larger temperatures below the Fermi energy, the gas enters the phase of a degenerate quantum gas. Therefore, the gas is modeled as a large collection of massive quantum-mechanical point particles occupying states of constant spin configurations I and s, interacting through two-body potentials given in equation (2.4). Single component gases will see all particles interact with each other equally, while gases consisting of mixtures of species - for instance fermions distinguished by spin - can have distinct interactions. Generally let us denote these conditions on atomic species by a tensor y_{nj} where n and j denote two atoms with some interaction relationship. The Hamiltonian in a coordinate system with the origin at the bottom of the trapping potential and interaction potential $V(r)$ from equation (2.4) is:

$$H_{\mathrm{total}} = \sum_{n=1}^{N} \left[-\frac{\hbar^2 \nabla_n^2}{2m} + \frac{1}{2} m \omega_{\mathrm{well}}^2 |\boldsymbol{r}_n|^2 \right] + \frac{1}{2} \sum_{n=1}^{N} \sum_{j \neq n}^{N} y_{nj} V(\boldsymbol{r}_n - \boldsymbol{r}_j). \tag{2.8}$$

The physical behaviour of the gas determined by the Hamiltonian in equation (2.8) is still rather complicated. For any given gas species it would be necessary to determine the interaction due to relative positions of molar amounts of atoms to describe the system, and solve a Schrödinger equation of order 10^{23} interacting particles. However it will be demonstrated in the following sections that ultra-cold degenerate quantum gases are universal: there exists another energy scale, dependant only on the s-wave scattering length a, at which all quantum degenerate gases obtain common features.

2.3 Two-body Scattering: Microscopic Level

The interaction between two atoms in a quantum gas modeled by equation (2.8) is determined by quantum mechanical scattering processes derived from the two-body interaction potentials of equation (2.4). Given that the potential is time-independent, the relative two-body scattering wavefunction ψ_{scatter} in the centre-of-

mass frame solves a time-independent Schrödinger equation [15]:

$$\left[-\frac{\hbar^2\nabla^2}{2m_{\text{rel}}} + V(\boldsymbol{r}) - E\right]\psi_{\text{scatter}}(\boldsymbol{r}) = 0. \tag{2.9}$$

where the relative distance $\boldsymbol{r} = \boldsymbol{r_i} - \boldsymbol{r}_j$ between two interacting atoms i, j while the mass m_{rel} is the reduced mass $\frac{m_i m_j}{m_i + m_j}$. This allows the treatment of the problem as a one-body interaction of a quantum-mechanical wave with a potential. The solution to the scattering wavefunction has asymptotically the form of a sum of a plane wave and a spherical wave modified by the effect of the potential $V(\boldsymbol{r})$ in the form of the scattering amplitude $f_k(\theta)$:

$$\psi_{\text{scatter}}(\boldsymbol{r}) \sim e^{ikz} + f_k(\theta)\frac{e^{ikr}}{r}. \tag{2.10}$$

The probability flux $\boldsymbol{j} = -\frac{i\hbar}{m}[\psi^*\nabla\psi - \psi\nabla\psi^*]$ is determined from the wavefunction $\psi_{\text{scatter}}(\boldsymbol{r})$. The differential cross-section is defined as the ratio of the radially scattered flux into an area $r^2 d\Omega$ to the incident flux of the plane wave:

$$\frac{d\sigma}{d\Omega} = |f_k(\theta)|^2. \tag{2.11}$$

The elastic scattering cross-section, a measure of the probability of particle scattering, is found as the integral of the differential cross-section over solid angle $d\Omega$ and relates to the scattering wave amplitude in general as

$$\sigma = \int |f_k(\theta)|^2 d\Omega = \int\int |f_k(\theta)|^2 \sin(\theta) d\theta d\varphi, \tag{2.12}$$

where integration occurs for the solid angle $d\theta$ in the interval 0 to π. However, in the case of identical particles there is interference between scattering amplitudes, and the integral need only evaluate angle θ from 0 to $\frac{\pi}{2}$:

$$\sigma = \int |f_k(\theta) \pm f_k(\pi - \theta)|^2 d\Omega, \tag{2.13}$$

where the constructive or destructive interference is distinguished by the scattering wavefunction being particle-exchange symmetric for identical bosons and antisymmetric for identical fermions.
If the potential $V(r)$ vanishes for large r, particles scattered by the potential will be observed as free particle waves far from the potential. Moving into the interaction picture, we let $V(r, t')$ be defined as

$$V(r, t') = e^{\frac{iH_0 t'}{\hbar}} V(r) e^{\frac{-iH_0 t'}{\hbar}}, \tag{2.14}$$

The time-evolution of states is performed by the unitary time-evolution operator $U(t, t_0)$, which satisfies the following nested integral equation:

$$\begin{aligned} U(t, t_0) &= U(t_0, t_0) - \int_{t_0}^{t} \frac{i}{\hbar} V(r, t') U(t', t_0) dt' \\ &= U(t_0, t_0) - \int_{t_0}^{t} \frac{i}{\hbar} V(r, t')[U(t_0, t_0) - \int_{t_0}^{t'} \frac{i}{\hbar} V(r, t'') U(t'', t_0) dt'']dt' ... \end{aligned}$$

By definition, $U(t_0, t_0) = 1$. We collect the integrals as time-ordered terms of an exponential series using the time-ordering operator $T\{\}$.

$$\begin{aligned} U(t, t_0) &= 1 - \int_{t_0}^{t} \frac{i}{\hbar} V(r, t')dt' + \int_{t_0}^{t}\int_{t_0}^{t} \frac{(-i)^2}{\hbar^2}\frac{1}{2!}V(r, t')V(r, t'')dt'dt''... \\ &= T\{\left[e^{-\frac{i}{\hbar}\int_{t_0}^{t} dt' V(r,t')}\right]\} \end{aligned}$$

The probability of an outgoing (+) scattered state with momentum $\boldsymbol{k}_\mathrm{i}$ and energy E_i, $|\psi^+_{\boldsymbol{k}_\mathrm{i}}(\boldsymbol{r}, t)\rangle = e^{-i\frac{E_\mathrm{i} t}{\hbar}}|\psi^+_{\boldsymbol{k}_\mathrm{i}}(\boldsymbol{r})\rangle$ being measured as a free plane wave with momentum $\boldsymbol{k}_\mathrm{f}$ and energy E_f at $t \to \infty$ is given by the scattering matrix $\mathcal{S}$ [16],

$$\mathcal{S} = \lim_{t\to\infty}[U(t, -\infty)] \tag{2.15}$$

$$= \lim_{t\to\infty}\lim_{\epsilon\to 0} T\{\left[e^{-\frac{i}{\hbar}\int_{-\infty+i\epsilon}^{t-i\epsilon} dt' V(r,t')}\right]\} \tag{2.16}$$

Evaluating on the incoming and outgoing states gives the elements:

$$\begin{aligned} \mathcal{S}_\mathrm{fi} &= \lim_{t\to\infty}\left[\lim_{\epsilon\to 0}\int d\boldsymbol{r'}^3 \psi^*_{\boldsymbol{k}_\mathrm{f}}(\boldsymbol{r'})U(t, -\infty)\psi^+_{\boldsymbol{k}_\mathrm{i}}(\boldsymbol{r'})\right] \\ &= \lim_{t\to\infty}[\lim_{\epsilon\to 0}\int d\boldsymbol{r'}^3 e^{-i\boldsymbol{k}_\mathrm{f}\cdot\boldsymbol{r'}} e^{\frac{i(E_\mathrm{f}-E_\mathrm{i})t}{\hbar}} e^{\epsilon t}\psi^+_{\boldsymbol{k}_\mathrm{i}}(\boldsymbol{r'})] \\ &= \delta^3(\boldsymbol{k}_\mathrm{f} - \boldsymbol{k}_\mathrm{i}) - 2\pi i\delta(E_\mathrm{f} - E_\mathrm{i})\mathcal{T}_\mathrm{fi}. \end{aligned}$$

The term $\mathcal{T}_\mathrm{fi}$ are the elements of the $\mathcal{T}$-matrix that represents the energy-conserving state transitions caused by the potential. In the momentum-space basis, the elements of $\mathcal{T}$ are related to the scattering amplitude $f_k(\theta)$, where θ is the angle between the initial and final momentum:

$$\mathcal{T} = \frac{4\pi\hbar^2}{m} f_k(\theta). \tag{2.17}$$

Therefore the differential cross-section is also expressible in terms of the $\mathcal{T}$-matrix:

$$\frac{d\sigma}{d\Omega} = \frac{m^2}{16\pi^2\hbar^4}|\mathcal{T}|^2.$$

And the total cross-section can be found as:

$$\sigma = \int \frac{m^2}{16\pi^2\hbar^4}|\mathcal{T}|^2 d\Omega. \tag{2.18}$$

The scattering amplitude $f_k(\theta)$ can be expanded into angular momentum components labeled by l. The partial wave expansion of the scattering amplitude is defined as:

$$f_k(\theta) = \sum_{l=0}^{\infty}(2l+1)f_l(k)P_l(\cos\theta). \tag{2.19}$$

Figure 2.1 indicates the plane wave expansion of the scattering wavefunction. The incident wavefunction contributions are the same as that of the free plane wave, but every outgoing l-wave is modified by a complex number $\mathcal{S}_l$. The numbers $\mathcal{S}_l$ are the eigenvalues of the $\mathcal{S}$-matrix in the basis of spherical harmonic functions. If the

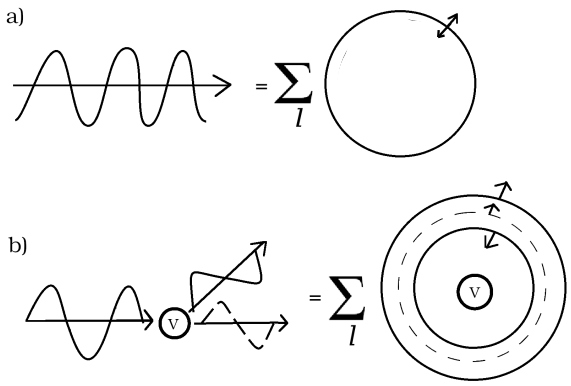

Figure 2.1: a) The plane wave expansion of e^{ikz} propagating in free space is asymptotically a sum of outgoing and incoming l-waves. b) Comparison of wave undergoing scattering (solid line) off potential V to plane wave in free space (dashed line). The incoming l-waves are not modified by the interaction while the outgoing l-waves are modified by a complex number $S_l \equiv 1 + 2ikf_l(k)$.

scattering is elastic, $|\mathcal{S}_l|^2 = 1$. Expanding ψ_{scatter} in the angular momentum basis gives a sum of radial wavefunctions $A_l(r)$,

$$\psi_{\text{scatter}}(r) = \sum_{l=0}^{\infty} i^l(2l+1)P_l(\cos\theta)A_l(r) \tag{2.20}$$

that has an asymptotic form for $r \to \infty$:

$$\psi_{\text{scatter}}(\boldsymbol{r}) \sim \frac{1}{2ik}\sum_{l=0}^{\infty}(2l+1)P_l(\cos\theta)((-1)^{l+1}\frac{e^{-ikr}}{r} + \mathcal{S}_l\frac{e^{ikr}}{r}). \tag{2.21}$$

Setting the partial wave expansion of (2.19) into equation (2.10) and comparing with equation (2.21), the partial wave amplitudes are related to $\mathcal{S}_l$:

$$f_l(k) = \frac{\mathcal{S}_l - 1}{2ik}. \tag{2.22}$$

$\mathcal{S}_l$ are represented as phase factors $e^{i2\delta_l}$ where δ_l are real-valued phase shifts of the outgoing l-waves. That gives an expression for each l partial wave amplitude $f_l(k)$:

$$f_l(k) = \frac{1}{k\cot\delta_l - ik}.$$

2.4 Low-energy limit for two-body scattering

For illustration, we use the hard sphere potential as an approximation of the interaction potential. Let:

$$V(r < l_{\text{vdW}}) = \infty, \qquad V(r > l_{\text{vdW}}) = 0.$$

The phase shifts are resolved depending on the solutions for the radial wavefunctions $A_l(r)$:

$$\left[\frac{\hbar^2(\partial_r^2+\frac{2}{r}\partial_r)}{2m_{\text{rel}}}-V(r)+\frac{\hbar^2(k^2-\frac{l(l+1)}{r^2})}{2m_{\text{rel}}}\right]rA_l(r)=0. \tag{2.23}$$

Outside the hard sphere, the radial component of the scattering wavefunction A_l is written in terms of the spherical functions [17]:

$$A_l(r)\approx e^{i\delta_l}(\frac{(kr)^l\cos(\delta_l)}{(2l+1)!!}+(2l-1)!!\frac{\sin(\delta_l)}{(rk)^{l+1}}). \tag{2.24}$$

Therefore at $A_l(r=l_{\text{vdW}})=0$,

$$\tan(\delta_l)\approx-\frac{(kl_{\text{vdW}})^{2l+1}}{(2l-1)!!(2l+1)!!} \tag{2.25}$$

In the low energy limit the most dominant scattering is from the $l=0$ s-waves as $\tan(\delta_0)$ reaches 0 with $k\to 0$ slowest:

$$\begin{aligned}f_k(\theta)&=\frac{1}{k}\sum_{l=0}^{\infty}(2l+1)e^{i\delta_l(k)}\sin(\delta_l(k))P_l(\cos(\theta))\\&=\frac{1}{k\cot\delta_0(k)-ik}+\mathcal{O}(k^2).\end{aligned}$$

The term $k\cot\delta_0(k)$ can be opened using the effective range expansion as a function of k^2 by using equation (2.25):

$$\begin{aligned}k\cot\delta_0(k)&\approx -k\frac{1}{kl_{\text{vdW}}}+\mathcal{O}(k^2),\\&:=-\frac{1}{a}+r_sk^2+\mathcal{O}(k^4).\end{aligned} \tag{2.26}$$

At those energies where k^2 is much smaller than effective range of scattering r_s, it is possible to approximate $k\to 0$ and then the scattering amplitude simplifies to

$$f_0=-a=-l_{\text{vdW}}. \tag{2.27}$$

The $\mathcal{T}$-matrix, and differential and total scattering cross-section become for identical bosons

$$\mathcal{T}=-\frac{8\pi\hbar^2a}{m},\qquad \frac{d\sigma}{d\Omega}=4|a|^2,\qquad \sigma=8\pi|a|^2,$$

and for distinguishable bosons

$$\mathcal{T}=-\frac{4\pi\hbar^2a}{m},\qquad \frac{d\sigma}{d\Omega}=|a|^2,\qquad \sigma=4\pi|a|^2.$$

The fact that at low energies the cross-section only depends on a justifies an effective field theory for the system that depends on this variable as a parameter. This is because the $\mathcal{T}$-matrix results in the effective field theory at that energy scale match exactly the effective-range expansion result - which in this case is only a dependence on a. To complete the argument, we step away from the l_{vdW}-dependent hard sphere potential representation and allow the potential to have an arbitrary, a-dependent shape that nonetheless appears as a simple delta-function in the low-energy limit.

2.5 Universality and the Efimov Effect

Ordinarily the scattering length a is of similar scale as the natural length scale l_{vdW}, but it can be manipulated with a magnetic by a mechanism known as a Feshbach resonance. Near resonance, the scattering length takes the form

$$a(B) = a_{\mathrm{bg}}(1 - \frac{\Delta_i}{B - B_i}), \tag{2.28}$$

where the bare scattering length a_{bg} is of order l_{vdW}, the parameter B_i is the Feshbach resonance point and $B = \Delta_i + B_i$ is the magnetic field strength for which the scattering length vanishes. Because a can be tuned to any size, the atomic interactions that depend on s-wave scattering can become very strongly repulsive or very strongly attractive, depending on the choice of magnetic field. For values of $|a|$ that greatly exceed l_{vdW}, the dominating effects of two-body scattering depend only on the scattering length a, atomic mass m, the spin statistic of the atomic species and the gas temperature T. For three-body scattering, a new parameter κ_* is necessary to account for the Efimov effect. The dependence of systems on these parameters to the exclusion of particular details of the interaction potentials or specific atomic properties is called universality. The primary parameter for universality can be considered the ratio of a to the natural length scale l_{vdW},

$$\mathtt{R} = \frac{l_{\mathrm{vdW}}}{|a|}, \tag{2.29}$$

and corrections to universality are of order $\mathcal{O}(\mathtt{R})$. Full universality is achieved in the following two limits that set $\mathtt{R} = 0$:

$$\begin{aligned} l_{\mathrm{vdW}} &\to 0, \\ \text{Unitary / Resonant limit: } a &\to \pm\infty. \end{aligned}$$

The Efimov effect is the name given to the realisation of a geometrically spaced energy spectrum of bound three-body states, known as trimers, which occurs if certain conditions for the masses, spin statistics and scattering lengths of the atoms are met [18]. When the conditions for the Efimov effect are met, the aforementioned parameter κ_* enters the theory in the form of the universal Efimov spectrum of the (n)th trimer branch in ascending order of depth, satisfied for large $|a|$, that follows equation 2.30:

$$-E_T^{(n)} = (e^{\frac{2\pi}{s_0}})^{n-n^*}\frac{\hbar^2\kappa_*^2}{m}, \tag{2.30}$$

where the constant s_0 depends on the mass ratios of the atomic species and their spin statistics. It will be shown in section 3.2.3 that this constant is the solution of a transcendental equation that determines the renormalization limit cycle of three-body scattering [19]. The parameter κ_* is a wavevector value that can be found from an arbitrarily shallow trimer in the spectrum for $n = n^*$, in the resonant limit. It is convenient to express this parameter as a term Λ_* found from the renormalization group limit cycle relationship:

$$s_0 \ln(|a|\Lambda_*) = [s_0 \ln(|a|\kappa_*) + 0.97] \bmod \pi \tag{2.31}$$

The result of the Efimov effect is a dependency of three-body observables such as three-body differential cross-sections on the scale of the system, and discrete scaling symmetries for these energy and length scales. Given a discrete scaling factor $\lambda = e^{\frac{\pi}{s_0}}$, the following discrete scaling symmetries apply to the system:

$$\Lambda_* \to \Lambda_* \qquad a \to \lambda^{-1} a \qquad \lim_{|a|\to\infty} E \to \lim_{|a|\to\infty} \lambda^2 E. \tag{2.32}$$

These scales affect the binding energies of the trimers in the resonant limit and certain characteristic lengths associated with them. Particularly the two-body scattering lengths associated to the thresholds of the bound three-body state system to the three atom system as well as the atom and two-body state system will be subject to this scaling as well. Such emergent universal bound state spectra - and their potential effects on scattering amplitudes - are also realisable in other systems of strongly interacting quantum degenerate gases.

3

Zero-Range Model: Effective Quantum Field Theory

In this chapter, an effective field theory known as the zero-range model will be constructed to describe the three-body interactions of degenerate quantum gases. Section 3.1 provides the derivation and renormalisation of the theory using the Feynman diagram formalism in the two-body sector for identical bosons. The solution of two-body scattering is directly implemented for the three-body sector in section 3.2 with the introduction of a two-particle field operator - the dimer - reducing the treatment with Feynman diagrams down to atom-dimer scattering as a two-body problem. Physical observables, such as the energy spectra for the three-particle bound states - known as trimers - and the atom-dimer scattering length, are described in section 3.3.

3.1 Two-Body Interactions

An effective field theory for ultracold atoms is built by replacing the detailed atom interaction potential $V(r)$ with an effective 2-body interaction $(\psi^\dagger\psi)^2$

$$H = \int d^3\boldsymbol{r} \left[\frac{1}{2m} \nabla\psi^\dagger \cdot \nabla\psi + \frac{\lambda_0}{4} (\psi^\dagger\psi)^2 \right], \tag{3.1}$$

for the case of two identical bosons, where λ_0 is a bare coupling coefficient of the theory. We have chosen units such that $\hbar = 1$. As a result, wavevectors denoted q, p, k are equivalent to momenta and frequencies $\omega_q, \omega_p, \omega$ are equivalent to energies. The dimensions of the fields ψ must satisfy the condition that the Hamiltonian has the dimension of energy. In the first term the dimension of $\frac{1}{m}$ is $[EL^2]$ and the Laplacian operator has dimension $[L^{-2}]$. This in turn means the fields ψ and $\psi^\dagger$ must have dimension $[L^{-\frac{3}{2}}]$ in order for the integration over dr^3 to yield a first term with dimension energy. The interaction term $(\psi^\dagger\psi)^2$ has dimension $[L^{-6}]$ and to compensate this the bare coupling coefficient must have dimension $[EL^3]$. Forthwith the exponent of the negative power of length for a field operator $\mathcal{O}_n(\psi, \psi^\dagger, \nabla\psi, \nabla\psi^\dagger)$ will be called the engineering dimension d_n.

$$\mathcal{O}_0 = \nabla\psi^\dagger \cdot \nabla\psi, \qquad d_0 = 5.$$
$$\mathcal{O}_1 = (\psi^\dagger\psi)^2, \qquad d_1 = 6.$$

The field operators are Fourier transforms of the ladder operators $\boldsymbol{a}, \boldsymbol{a}^\dagger$ of the quantum-mechanical harmonic oscillator:

$$\psi(\boldsymbol{r}) = \frac{1}{(2\pi)^3}\int \boldsymbol{a_k} e^{-i\boldsymbol{k}\cdot\boldsymbol{r}} d^3\boldsymbol{k}$$
$$\psi^\dagger(\boldsymbol{r}) = \frac{1}{(2\pi)^3}\int \boldsymbol{a}_{\boldsymbol{k}}^\dagger e^{i\boldsymbol{k}\cdot\boldsymbol{r}} d^3\boldsymbol{k}$$

and therefore act on spaces of coherent states, which are superpositions of harmonic oscillator eigenstates [20]. To describe particle scattering, the time-independent operators $\psi^\dagger, \psi$ are transformed into the interaction picture.

$$\psi \to \psi(\boldsymbol{r}, t) = e^{iH_0 t}\psi e^{-iH_0 t} \tag{3.2}$$
$$H \to H_{0,I} + H_I = \int d\boldsymbol{r}^3 \frac{1}{2m}\nabla\psi^\dagger(\boldsymbol{r}, t)\cdot\nabla\psi(\boldsymbol{r}, t) + \frac{\lambda}{4}(\psi^\dagger(\boldsymbol{r}, t)\psi(\boldsymbol{r}, t))^2 \tag{3.3}$$

Because $H_0 = \int d^3\boldsymbol{r}\frac{1}{2m}\nabla\psi^\dagger\cdot\nabla\psi$ is time-independent, the unitary time-evolution operators $e^{\pm iH_0 t}$ commute with H_0, therefore $H_0 = H_{0,I}$.

3.1.1 The $\mathcal{S}$-matrix in the Interaction Picture

The $\mathcal{S}$-matrix unitary operator will determine the evolution of the incoming states into the outgoing states:

$$\mathcal{S}_{\text{fi}} = \langle\psi^-(\boldsymbol{r}, t)|\psi^+(\boldsymbol{r}, t)\rangle \tag{3.4}$$

So in the basis of coherent states:

$$\mathcal{S}_{\text{fi}} = \langle \text{f}|e^{iH_0 t}e^{-iH(t-t')}e^{-iH_0 t'}|\text{i}\rangle \tag{3.5}$$

The operator $\mathcal{S}(t, t') = e^{iH_0 t - iH(t-t')}e^{-iH_0 t'}$ may be differentiated in final time t:

$$\frac{d}{dt}\mathcal{S}(t, t') = -ie^{iH_0 t}Ve^{-iH_0 t}e^{iH_0 t - iH(t-t')}e^{-iH_0 t'} = -iV_I(t)\mathcal{S}(t, t') \tag{3.6}$$

where V_I is the interaction potential operator in the interaction picture which in our field theory matches $H_\text{I} = H - H_0$ presented in equation (3.3). $\mathcal{S}(t', t') = 1$ is the identity of a state at a given time, so the integral equation of $\mathcal{S}$ can be formed as

$$\begin{aligned}\mathcal{S}(t, t') &= 1 - i\int_{t'}^{t} H_\text{I}(t'')\mathcal{S}(t'', t')dt'' \\ &= 1 - i\int_{t'}^{t} H_\text{I}(t'')[1 - i\int_{t'}^{t''} H_\text{I}(t''')\mathcal{S}(t''', t'')]dt''dt''' \\ &= 1 - i\int_{t'}^{t} H_\text{I}(t'')[1 - i\int_{t'}^{t''} H_\text{I}(t''')[1 - i\int_{t'}^{t'''} H_\text{I}(t''')\mathcal{S}(t'''', t''')]]dt''dt'''dt''''...\end{aligned}$$

And so on indefinitely. This can be expressed as an infinite sum of interaction Hamiltonians, known as the Dyson series, and evaluated at infinitely distant points from the interaction:

$$\mathcal{S}(\infty, -\infty) = 1 - i\int_{t'}^{t} H_\text{I}(t'')dt'' + (-i)^2\int_{t'}^{t}\int_{t'}^{t''} H_\text{I}(t'')H_\text{I}(t''')dt''dt''' + ...$$

Let time-ordering operator $T\{\}$ be defined using the Heaviside step-function, which ensures only the correct time order term is respected in the result:

$$\begin{aligned} T\{f(\boldsymbol{r}_1,t_1)\} &= f(\boldsymbol{r}_1,t_1) \\ T\{f_1(\boldsymbol{r}_1,t_1)f_2(\boldsymbol{r}_2,t_2)\} &= \Theta(t_1-t_2)f_1(\boldsymbol{r}_1,t_1)f_2(\boldsymbol{r}_2,t_2)+\Theta(t_2-t_1)f_2(\boldsymbol{r}_2,t_2)f_1(\boldsymbol{r}_2,t_1) \\ T\{\prod_{n=1}^{N} f_n(\boldsymbol{r}_n,t_n)\} &= \text{ Sum of permutations of } f_n(\boldsymbol{r}_n,t_n) \text{ times product of } \Theta(t_n-t_{n'}) \end{aligned}$$

As the sum of permutations will have $N!$ options of time-ordering included as terms, the Dyson series is factored by $\frac{1}{N!}$.

$$\begin{aligned} \mathcal{S}(\infty,-\infty) &= 1+\sum_{N=1}^{\infty}\frac{1}{N!}(-i)^N\prod_{n=1}^{N}T\{\int_{-\infty}^{\infty}dt_{(n)}H_{\mathrm{I}}(t_n)\} \\ &= 1+\sum_{N=1}^{\infty}\frac{1}{N!}(-i)^N\int_{-\infty}^{\infty}\prod_{n=1}^{N}dt_n\int\prod_{n=1}^{N}d^3\boldsymbol{r}_nT\{\prod_{n=1}^{N}V_{\mathrm{I}}(\boldsymbol{r}_n,t_n)\} \end{aligned}$$

In this theory the interaction potential $V_{\mathrm{I}}(\boldsymbol{r}_n,t_n)$ will be composed of a sum of products of field operators $\psi(\boldsymbol{r}_n,t_n)$ and $\psi^\dagger(\boldsymbol{r}_n,t_n)$.
In order to act with the $\mathcal{S}$ operator on any initial and final states, it is possible to commute/anticommute the field operators constituting V_I such that all creation operators will be acting on $\langle \mathrm{f}|$ and all annihilation operators will be acting on $|\mathrm{i}\rangle$. In the bosonic case, each such commutation between creation/annihilation operators at $(\boldsymbol{r}_n,t_n)$ to annihilation/creation operators at $(\boldsymbol{r}_{n'},t_{n'})$ will add $\delta^3(\boldsymbol{r}_n-\boldsymbol{r}_{n'})$. Because the final and initial states are themselves expressible as creation and annihilation operators acting on vacuum states $|0\rangle$ and $\langle 0|$, with prefactors $e^{\pm i(\boldsymbol{r}_{\mathrm{f,i}}\cdot\boldsymbol{k}_{\mathrm{f,i}}-t_{\mathrm{f,i}}\omega_{\mathrm{f,i}})}$ those operators may also be commuted until all creation and annihilation operators are acting on vacuum. By Wick's theorem, only the δ-functions that were used to perform this normal-ordering procedure will remain, factored by the coupling constants and subject to the time-ordering Heaviside step-functions. These δ-functions are collected into the time-ordering of creation and annihilation operator pairs, which constitute the retarded propagators in position space:

$$\begin{aligned} T\{\psi^\dagger(\boldsymbol{r}_n,t_n),\psi(\boldsymbol{r}_{n'},t_{n'})\} &= \Theta(t_n-t_{n'})(\psi(\boldsymbol{r}_{n'},t_{n'})\psi^\dagger(\boldsymbol{r}_n,t_n)+\delta^3(\boldsymbol{r}_n-\boldsymbol{r}_{n'})) \\ &\quad+\Theta(t_{n'}-t_n)\psi(\boldsymbol{r}_{n'},t_{n'})\psi^\dagger(\boldsymbol{r}_n,t_n) \\ \Theta(t_n-t_{n'})\delta^3(\boldsymbol{r}_n-\boldsymbol{r}_{n'}) &= D_R(\boldsymbol{r}_n-\boldsymbol{r}_{n'},t_n-t_{n'}) \end{aligned}$$

The $\mathcal{S}_{\mathrm{fi}}$ matrix for the theory determined by the Hamiltonian in equation (3.1) is then expressible in position space as

$$\begin{aligned} \mathcal{S}_{\mathrm{fi}} = \delta_{\mathrm{fi}} + \langle 0|\sum_{N=1}^{\infty}\frac{1}{N!}(\frac{-i}{4})^N\lambda^N M_N\int_{-\infty}^{\infty}\prod_{n=1}^{N}dt_n\int\prod_{n=1}^{N}d^3\boldsymbol{r}_n \\ \prod_{n,n'}D_R(\boldsymbol{r}_n-\boldsymbol{r}_{n'},t_n-t_{n'})\times e^{-i(\boldsymbol{r}_i\cdot\boldsymbol{k}_i-t_i\omega_i)}e^{i(\boldsymbol{r}_{\mathrm{f}}\cdot\boldsymbol{k}_{\mathrm{f}}-t_{\mathrm{f}}\omega_{\mathrm{f}})}|0\rangle. \end{aligned}$$

The first δ_{fi} term does not contribute to interactions, and subtracting it produces the $i\mathcal{T}_{\mathrm{fi}}$ transition matrix. Only fully connected products of propagators contribute

to the transition matrix, that is from starting $n' = \mathrm{i}$ to final $n = \mathrm{f}$ all interrim n', n must form causal paths from i to f. The term M_N results as the possible distinct permutations of propagator products are added. Each vertex may be permuted with any other, leading to $N!$ sets of permutations of propagator products. For an interaction of two creation and two annihilation field operators at each vertex, it is possible to permute each field twice, leading to $(2!)^2 = 4$ sets of propagator product terms for each vertex, 4^N. However, such exchanges are not distinct if the internal propagators between vertices are identical, leading to the emergence of a symmetry factor $S_2 = 2$ in the case of identical bosons:

$$i\mathcal{T}_{fi} = \langle 0| \sum_{N=1}^{\infty} (\frac{-i\lambda}{S})^N \int_{-\infty}^{\infty} \prod_{n=1}^{N} dt_n \int \prod_{n=1}^{N} d^3\boldsymbol{r}_n \prod_{n,n'}^{\text{distinct}} D_R(\boldsymbol{r}_n - \boldsymbol{r}_{n'}, t_n - t_{n'}) e^{-i(\boldsymbol{r}_i \cdot \boldsymbol{k}_i - t_i\omega_i)} e^{i(\boldsymbol{r}_f \cdot \boldsymbol{k}_f - t_f\omega_f)} |0\rangle$$

In momentum space, Fourier transformation yields the following result for the scattering amplitude $\mathcal{A}$ of the interaction leading from initial to final coherent states:

$$\begin{aligned} i\mathcal{T}_{\mathrm{fi}} &= \langle 0| \sum_{N=1}^{\infty} (\frac{-i\lambda}{S})^N \prod_{n,n'}^{\text{distinct}} D_R(\boldsymbol{k}_n - \boldsymbol{k}_{n'}, \omega_n - \omega_{n'}) |0\rangle \delta^3(\boldsymbol{k}_{\mathrm{f}} - \boldsymbol{k}_{\mathrm{i}}) \delta(\omega_{\mathrm{f}} - \omega_{\mathrm{i}}) \\ &\equiv i\mathcal{A}(\boldsymbol{k}_{\mathrm{f}}, \boldsymbol{k}_{\mathrm{i}}, \omega_{\mathrm{f}}, \omega_{\mathrm{i}}) \times \delta^3(\boldsymbol{k}_{\mathrm{f}} - \boldsymbol{k}_{\mathrm{i}}) \delta(\omega_{\mathrm{f}} - \omega_{\mathrm{i}}) \end{aligned}$$

3.1.2 The Scattering Amplitude: Green's Function and Feynman Diagrams

In momentum space, the free atom propagator becomes with $+i\epsilon$ provided by the Heaviside step-functions in time ensuring it has the properties of a retarded propagator,

$$D_{\psi,\psi^\dagger}(q, \omega_q) = \frac{i}{\omega_q - \frac{q^2}{2m} + i\epsilon}. \tag{3.7}$$

We can confirm that this is consistent with the retarded propagator in position space through Fourier transform:

$$F[D_{\psi,\psi^\dagger}(q, \omega_q)] = \int \frac{dq^3}{(2\pi)^3} \int_{-\infty}^{\infty} \frac{d\omega}{2\pi} \frac{e^{-i\omega(t_2 - t_1)} e^{iq(\boldsymbol{r}_2 - \boldsymbol{r}_1)}}{\omega_q - \frac{q^2}{2m} + i\epsilon} \tag{3.8}$$

which after a shift $\omega \to \omega + \frac{p^2}{2m}$ gives a weighted Heaviside step-function from its integral representation:

$$F[D_{\psi,\psi^\dagger}(q, \omega_q)] = \Theta(t_2 - t_1) \int \frac{dq^3}{(2\pi)^3} e^{iq(\boldsymbol{r}_2 - \boldsymbol{r}_1)} e^{-i(\frac{q^2}{2m} - i\epsilon)(t_2 - t_1)}$$

where after the limit $\epsilon \to 0$ is taken the terms within the integral collect into plane waves of type $\frac{e^{iq\boldsymbol{r}_n - i\frac{q^2}{2m}t_n}}{(2\pi)^{\frac{3}{2}}}$ and succinctly become delta functions $\delta^3(\boldsymbol{r}_2 - \boldsymbol{r}_1)$ upon integration for all q due to the orthonormality of these functions.

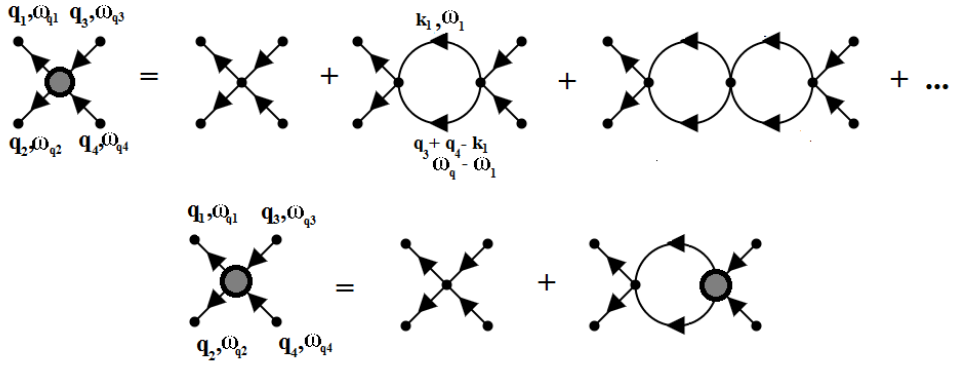

Figure 3.1: The fully connected two-body Green's function in momentum space $i\mathcal{A}_2$ is built up from a sum of contributions at each loop level. To form an additional loop, the previous diagram in the iteration must be connected to a new vertex with two additional propagators. Lower diagram shows the Green's function as the Lippmann-Schwinger equation.

In addition to the free propagator it is necessary to determine the tree-level 4-point vertex. It is found as the $N = 1$ term of the sum in the $\mathcal{T}_{fi}$ matrix. In momentum space the first order vertex of a 2-body interaction at 0 loop level becomes:

$$\mathcal{F}^0_{\psi^\dagger\psi^\dagger,\psi\psi} = -ic_1\lambda_0, \tag{3.9}$$

where $c_1 = 1$ for identical bosons. The Feynman rules for two-body scattering are shown in appendix A.1, figure A.1.
The only fully-connected way to construct the contributing amplitudes to two-body scattering is shown diagrammatically in figure 3.1.
To obtain the interaction at all loop levels, the contributions must be summed over to infinite number of loops to produce the fully connected and amputated two-body interaction diagram $i\mathcal{A}_2$:

$$i\mathcal{A}_2 = -\lambda_0 c_1 \left(1 - \lambda_0 c_{12} \int \frac{dk^3}{(2\pi)^3} \int_{-\infty}^{\infty} \frac{d\omega}{2\pi} \left[\frac{i}{\omega - \frac{k^2}{2m} + i\epsilon} \frac{i}{(\omega_q - \omega) - \frac{(q_3+q_4-k)^2}{2m} + i\epsilon)}\right]\right)^{-1}. \tag{3.10}$$

A symmetry term $c_{12} = \frac{c_1}{2} = \frac{1}{2}$, the result of exchangeable internal propagators in figure 3.1, is included for identical bosons. For distinguishable bosons, the symmetry factor is $c_1 = c_{12} = \frac{1}{4}$ due to the non-symmetry of the tree-level diagram and the internal propagators not being interchangeable.
Let $I_\omega = \int_{-\infty}^{\infty} \frac{d\omega}{2\pi} [\frac{i}{\omega - \frac{k^2}{2m} + i\epsilon} \frac{i}{(\omega_q - \omega) - \frac{(q_3+q_4-k)^2}{2m} + i\epsilon)}]$. The contour integration over frequency ω to simplify the propagator loop is demonstrated in figure 3.2. Start by changing the integration variable from real ω to complex z:

$$I_\omega = \left[\oint \frac{dz}{2\pi} \frac{i}{z - (\frac{k^2}{2m} - i\epsilon)} \frac{-i}{z - (\omega_q - \frac{(q_3+q_4-k)^2}{2m} + i\epsilon)} - \int_C \frac{dz}{2\pi} \frac{i}{z - (\frac{k^2}{2m} - i\epsilon)} \frac{-i}{z - (\omega_q - \frac{(q_3+q_4-k)^2}{2m} + i\epsilon)}\right]$$

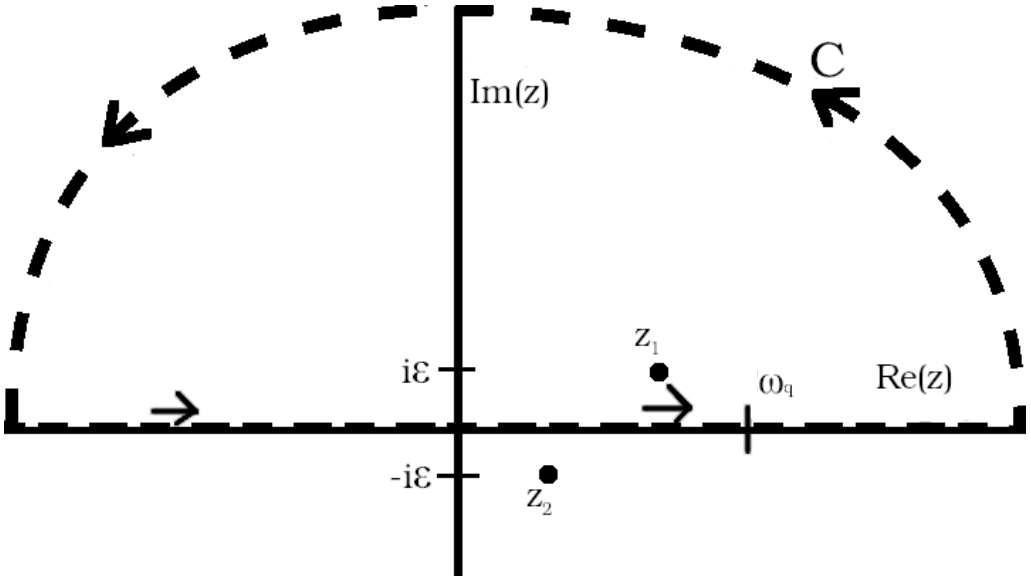

Figure 3.2: Contour integral over the complex frequency plane in counterclockwise orientation for looped-propagator factor. The propagator product has poles at $z_1 = \omega_q - \frac{(q_3+q_4-k)^2}{2m} + i\epsilon$ in the upper half plane and $z_2 = \frac{k^2}{2m} - i\epsilon$ in the lower half plane. The contour encloses only pole z_1 and can be found as its residual. The integral over the real axis equates the contour integral as the contribution from the semicircular path C vanishes for large radius of C.

The integral along the far curve C vanishes due to the contribution of the curve length being diminished by the value of the denominator as $|z| \to \infty$, meaning the contour integral equates the real line integral. Then the Residue theorem can be used to evaluate the contour integral over the upper plane pole.

$$\begin{aligned} I_\omega &= \frac{2\pi i}{2\pi} \lim_{z \to (\omega_q - \frac{(q_3+q_4-k)^2}{2m} + i\epsilon)} (z - (\omega_q - \frac{(q_3+q_4-k)^2}{2m} + i\epsilon)) \\ &\quad \times [\frac{1}{z - (\frac{k^2}{2m} - i\epsilon)} \frac{1}{z - (\omega_q - \frac{(q_3+q_4-k)^2}{2m} + i\epsilon)}] \\ &= \frac{i}{\omega_q - \frac{(k - \frac{q_3+q_4}{2})^2}{m} - \frac{(q_3+q_4)^2}{4m} + i\epsilon} \end{aligned}$$

Setting I_ω back into $i\mathcal{A}_2$, the result for the scattering amplitude of identical bosons is:

$$\mathcal{A}_2 = -\lambda_0 \left(1 - \frac{\lambda_0}{2} \int \frac{dk^3}{(2\pi)^3} \frac{1}{\omega_q - \frac{(k - \frac{q_3+q_4}{2})^2}{m} - \frac{(q_3+q_4)^2}{4m} + i\epsilon}\right)^{-1}. \tag{3.11}$$

Denote the integral part as I_2. Because this integral is divergent, an ultraviolet regularization scheme must be used to compute it. The ultraviolet cutoff of the momentum Λ is according to the scaling limit an inverse of the natural length scale, which in this case is the van der Waals length, so $\Lambda \sim \frac{1}{l_{\mathrm{vdW}}}$. Before introducing the cutoff, first factor the mass out of the momentum terms in the denominator, and

collect the terms as such:

$$I_2 = \int \frac{dk^3}{(2\pi)^3} \frac{-m}{(k - \frac{q_3+q_4}{2})^2 + (\sqrt{(\frac{q_3+q_4}{2})^2 - \omega_q m - i\epsilon})^2}$$

After a variable change $y = k - \frac{q_3+q_4}{2}$, it is possible to change the evaluation into a spherical integral and impose an ultraviolet cutoff condition $\infty \to \Lambda$:

$$I_2 = -\frac{m}{(2\pi)^3} 4\pi \int_0^\Lambda dy \frac{y^2}{y^2 + (\sqrt{(\frac{q_3+q_4}{2})^2 - \omega_q m - i\epsilon})^2}$$

the integral is completed through addition of zero $\frac{x^2}{x^2+f(x)} = \frac{x^2+f(x)}{x^2+f(x)} - \frac{f(x)}{x^2+f(x)}$:

$$I_2 = -\frac{m}{2\pi^2} \left[\Lambda - \frac{(\sqrt{(\frac{q_3+q_4}{2})^2 - \omega_q m - i\epsilon})^2}{\sqrt{(\frac{q_3+q_4}{2})^2 - \omega_q m - i\epsilon}} \times \arctan\left(\frac{(\Lambda - \frac{q_3+q_4}{2})}{\sqrt{(\frac{q_3+q_4}{2})^2 - \omega_q m - i\epsilon}}\right) \right].$$

It should be supposed that the ultraviolet cutoff Λ is far greater than any energy scale reached by two-body scattering in the ultra-cold regime. The arctan term can be simplified to $\arctan(\infty) = \frac{\pi}{2}$. Abreviate $\Delta^2 = (\frac{q_3+q_4}{2})^2 - \omega_q m - i\epsilon$, then denoting this 2-loop integral as $I_2(q_3 + q_4, \omega_q)$ gives:

$$I_2(q_3 + q_4, \omega_q) = -\frac{m}{2\pi^2}[\Lambda - \frac{\pi}{2}\Delta]. \tag{3.12}$$

Therefore the off-shell scattering amplitude is

$$\mathcal{A}_{\text{id, boson}}(\omega_q, q_3, q_4) = -\left[\frac{1}{\lambda_0} + \frac{m}{4\pi^2}\Lambda - \frac{m}{8\pi}\Delta\right]^{-1}, \tag{3.13}$$

$$\mathcal{A}_{\text{general boson}}(\omega_q, q_3, q_4) = -\left[\frac{4}{\lambda_0} + \frac{m_\text{r}}{\pi^2}\Lambda - \frac{m_\text{r}}{2\pi}\Delta\right]^{-1}, \tag{3.14}$$

where m_r is the reduced mass of the distinguishable bosons, $m = 2m_\text{r}$ if the masses are identical. The equations (3.13) and (3.14) simplify by performing a transformation of the energy and momenta into the center-of-mass frame which sets $q_{3\text{cm}} + q_{4\text{cm}} = 0$ so that $\Delta^2_{\text{cm}} = -\omega_{q\text{cm}} m - i\epsilon$. The on-shell amplitude that corresponds to a limitation of the energy to the case where the sum of the energy is equal to the total kinetic energy of the particles, that is the total energy sufficient for these two atoms to exist with given momenta q_3, q_4. Set ω_q to be the threshold energy:

$$\omega_q = \frac{q_3^2}{2m} + \frac{q_4^2}{2m} = \frac{q^2}{m}. \tag{3.15}$$

Evaluating the amplitude for this energy will give the $\mathcal{T}(\omega_q, q_1, q_2, q_3, q_4)$ transition matrix element:

$$\mathcal{T}_{\text{zero range}} = \mathcal{A}_2 \delta(\frac{q^2}{m} - (\omega_{q1} + \omega_{q_2}))\delta^3(q_3 + q_4 - q_1 - q_2). \tag{3.16}$$

3.1.3 Renormalisation of the Two-Body Coupling Coefficient

The renormalisation condition can be formulated so that in the low energy limit of $q^2 \to 0$, the result should be exactly the same as the result of quantum mechanical scattering at low energy in the scaling limit $l_{\text{vdW}} \to 0$, such that all terms of the effective range expansion in section 2.3, equation (2.26) of $k \cot \delta_0(k)$ were eliminated aside from $-\frac{1}{a}$.

$$\begin{aligned}
\mathcal{T}_{\text{scatter}} &= \lim_{q^2 \to 0} [\mathcal{T}_{\text{zero range}}] \\
-\frac{8\pi}{m} a &= \lim_{q^2 \to 0} -[\frac{1}{\lambda_0} + \frac{m}{4\pi^2}\Lambda - \frac{m}{8\pi}(-q^2)^{\frac{1}{2}}]^{-1} \\
a &= \frac{m}{8\pi}[\frac{1}{\lambda_0} + \frac{m}{4\pi^2}\Lambda]^{-1}
\end{aligned}$$

This gives an explicit definition of the bare coupling coefficient in terms of scattering length:

$$\lambda_0 = \frac{8\pi a}{m}[1 - \frac{2a}{\pi}\Lambda]^{-1} \tag{3.17}$$

Reinsert these expressions into the expression of the $\mathcal{T}_{\text{zero range}}$ matrix:

$$\lim_{\epsilon \to 0} \mathcal{T}_{\text{zero range}} = \frac{8\pi a}{m(iaq - 1)}, \left(\text{or } \frac{4\pi a}{m(iaq - 1)} \right). \tag{3.18}$$

Scale-invariant fix-points of a can be found for the zero-range Hamiltonian with the definition of new constants:

$$\hat{C}_1 = \frac{\Lambda}{4}\frac{8\pi a}{m}[1 - \frac{2a}{\pi}\Lambda]^{-1}. \tag{3.19}$$

The meaning of the running constant is such that the differential equation

$$\Lambda \frac{d}{d\Lambda}\hat{C}_1 = \beta(\hat{C}_1), \tag{3.20}$$

maps out the possible $\hat{C}_1$ as a trajectory of Λ, which can be viewed as the variety of Hamiltonian theories depending on the choice of cutoff, or scale. A fix-point in this trajectory where $\hat{C}_1$ is independent of Λ represents a scale-invariant Hamiltonian with the coupling defined at that fixed point. The fix-point of $\hat{C}_1$ in turn gives the values of scattering length a at which theory is scale-invariant. The two factors now determine the solutions for when $\beta(\hat{C}_1) = 0$, which are the fixpoints of the renormalisation group flow and therefore correspond to a scale-invariant Hamiltonian:

$$\begin{aligned}
\frac{2a\Lambda}{\pi - 2a\Lambda} &= 0 && \to a = 0 \\
\frac{2a\Lambda}{\pi - 2a\Lambda} &= \frac{1}{\frac{\pi}{2a\Lambda} - 1} = \frac{1}{-1} && \to a = \pm\infty
\end{aligned}$$

The theory is therefore scale invariant in the non-interactive case $a = 0$ and the resonant limit $|a| \to \infty$. Because the theory is dependent exclusively on the length scale of a, it must treat the interaction potential as contact through the s-wave scattering channel. This consequence of the scaling limit gives the model its zero-range property.

3.2 Three-Body Interactions

In order to produce low-energy three-body interactions, it is userful to rewrite the Hamiltonian in equation (3.1) with quantum field operators Ψ signifying the presence of two-atom bound states, known as dimer fields, with the two-body dimer-atom interaction bare coupling constant γ_0. In the case of two identical boson species this will be:

$$H = \int d\boldsymbol{r}^3 \left[\frac{1}{2m} \nabla\psi^\dagger \cdot \nabla\psi - \frac{\lambda_0}{4}\Psi^\dagger\Psi + \frac{\lambda_0}{4}(\Psi^\dagger\psi\psi + \psi^\dagger\psi^\dagger\Psi) + \frac{\gamma_0}{36}\Psi^\dagger\psi^\dagger\Psi\psi \right]. \quad (3.21)$$

The dimer fields are not independent from the atomic fields, as they are subjected to the constraints:

$$\begin{aligned} 0 &= \frac{\lambda_0}{4}\Psi - \frac{\lambda_0}{4}\psi\psi - \frac{\gamma_0}{36}\psi^\dagger\Psi\psi, \\ \Psi &= \frac{\psi\psi}{1 - \frac{\gamma_0}{9\lambda_0}\psi^\dagger\psi}. \end{aligned}$$

Therefore if the dimer-atom coupling constant $\gamma_0 = 0$, the dimer field is the product of two atomic fields. With this definition of the dimer field, up to a truncation to the three-body sector the Hamiltonians in equation (3.21) is the zero-range Hamiltonians in equation (3.1) with the added terms $\frac{\gamma_0}{36}(\psi^\dagger\psi)^3$ or $\frac{\gamma_0}{36}(\psi^\dagger_{1\uparrow}\psi_{1\uparrow})^2(\psi^\dagger_{2\downarrow}\psi_{2\downarrow})$ respectively. This means it is an adequate effective field theory for three-body interactions under the condition that the two-body dimer exists and its threshold energy is within the low-energy limit. The free particle propagator for the atom is the same as in the two-body model, $D_{\psi,\psi^\dagger}(q,\omega_q)$. A bare, non-causal propagator is introduced for the dimer field by the self-interaction term $\frac{\lambda_0}{4}(\Psi^\dagger\Psi)$:

$$D^0_{\Psi,\Psi^\dagger} = \frac{4i}{\lambda_0}, \quad (3.22)$$

which in fact is 4 times the inverse of the vertex of two-body interaction $\mathcal{F}^0_2$. The recombination interactions are represented at the tree level by three-point vertices:

$$\mathcal{F}^0_{2\psi^\dagger,\Psi} = \mathcal{F}^0_{\Psi^\dagger,2\psi} = -i\frac{\lambda_0}{2}, \quad (3.23)$$

and the dimer-atom scattering is represented by the four-point vertex:

$$\mathcal{F}^0_{\Psi^\dagger,\psi^\dagger,\psi,\Psi} = -i\frac{\gamma_0}{36}. \quad (3.24)$$

The factor $\frac{1}{2} = \frac{2}{4}$ in the three-point vertex occurs as the diagrams are symmetric under exchange of atom fields in the exchange of identical bosons. The four-point vertex has no symmetry and the factor $\frac{1}{36}$ persists from the definition of the interaction Hamiltonian.

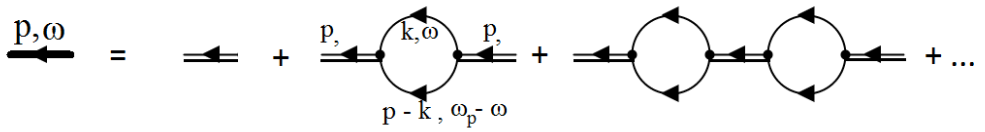

Figure 3.3: The exact boson dimer propagator is found diagrammatically. For each loop level the contributing diagram is multiplied by an additional pair of decay and formation 3-point vertices and two looped atom propagators which are integrated over all indeterminate momenta and energies. Each loop level has a symmetry factor $\frac{1}{2}$. The propagator loop integral is computed exactly as in equation (3.12) to be $I_2(p,\omega_p) = -\frac{m}{2\pi^2}[\Lambda - \frac{\pi}{2}\sqrt{(\frac{p^2}{4} - \omega_p m - i\epsilon)}]$. The general case is analogously determined with the mass m replaced with double of the reduced mass $2m_\mathrm{r}$.

3.2.1 The Exact Dimer Propagator

The $\mathcal{T}$-matrix receives ultraviolet-divergent contributions to the exact propagator for the diatomic field from the products of the recombination diagrams. These ultraviolet-divergent contributions are identical to the ultraviolet divergence of the two-body scattering amplitude $i\mathcal{A}_2$ developed in section 3.1, which was proven to be renormalisable using ultraviolet cutoff regularization scheme, because they are represented by equivalent diagrams. The exact propagator shown in figure 3.3 to form an infinite geometric series. In the general case of mass ratios, the mass is replaced according to $\frac{m}{2} \to m_\mathrm{r}$ during the internal ω contour integral evaluation:

$$iD_{\Psi,\Psi^\dagger;m}(p,\omega_p) = i\frac{4}{\lambda_0} + \frac{1}{2}(i\frac{4}{\lambda_0})^2(\frac{-i\lambda_0}{2})^2 iI_2(p,\omega_p;m) + \frac{1}{4}(i\frac{4}{\lambda_0})^3(\frac{-i\lambda_0}{2})^4(iI_2(p,\omega_p;m))^2 + \ldots$$

$$\begin{aligned} D_{\Psi,\Psi^\dagger;m}(p,\omega_p) &= \frac{4}{\lambda_0}\sum_{n=0}^{\infty}\left[\frac{\lambda_0}{2}I_2(p,\omega_p;m)\right]^n \\ &= \frac{4}{\lambda_0}\left(1 + \frac{\lambda_0}{2}\frac{m}{2\pi^2}[\Lambda - \frac{\pi}{2}\sqrt{(\frac{p^2}{4} - \omega_p m - i\epsilon)}]\right)^{-1} \end{aligned}$$

The bosonic dimer propagator's renormalisation utilizes the same renormalization condition as the two-body scattering amplitude because the combined diagram $\mathcal{F}^0_{2\psi^\dagger,\Psi} D_\Psi \mathcal{F}_{\Psi^\dagger,2\psi} \sim \mathcal{A}_2$. Therefore with $\lambda_0 = \frac{8\pi a}{m}[1 - \frac{2a}{\pi}\Lambda]^{-1}$:

$$D_{\Psi,\Psi^\dagger}(p,\omega_p;m) = \left(\frac{8\pi a}{4m(1-\frac{2a}{\pi}\Lambda)^2} - \frac{\lambda_0^2 m}{32\pi}\sqrt{(\frac{p^2}{4} - \omega_p m - i\epsilon)}\right)^{-1}, \tag{3.25}$$

and factoring out λ_0 gives

$$D_{\Psi,\Psi^\dagger}(p,\omega_p;m) = \frac{32\pi}{\lambda_0^2}\left(\frac{m}{a} - m\sqrt{(\frac{p^2}{4} - \omega_p m - i\epsilon)}\right)^{-1}. \tag{3.26}$$

The dimer exists only when the scattering length $a > 0$. Then the dimer's self-energy $E_{2\Psi}$ is the pole of this propagator, which is at $\omega_p = \frac{p^2}{4m} - \frac{1}{ma^2} + i\epsilon$ and lies in

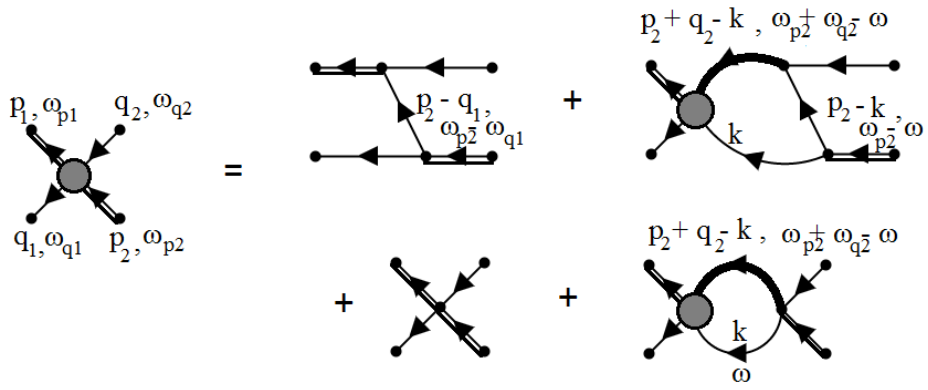

Figure 3.4: The integral equation of Green's function $\mathcal{A}_3$ is formed by representing all looped terms as the tree terms connected to the Green's function by propagators of undetermined energy and momenta. The recombination vertices diagram has two undetermined atomic propagators and one undetermined diatomic propagator as part of the loop, while the four-point vertex diagram has one of each undetermined propagator.

the upper half complex plane. It's possible to define a field renormalisation constant Z_Ψ:

$$Z_\Psi = \frac{64\pi}{\lambda_0^2 a m^2}$$

The field renormalisation constant is applied to create this definition of the exact propagator:

$$D_{\Psi,\Psi^\dagger}(p,\omega_p;m) := Z_\Psi \frac{am^2}{2} \frac{1}{\frac{m}{a} - m\sqrt{(\frac{p^2}{4} - \omega_p m - i\epsilon)}} \tag{3.27}$$

Together with the vertices and atomic propagator, the exact dimer propagator serves as the building element for the Feynman diagrams of this effective field theory. The Feynman rules for this approach to three-body scattering are shown in appendix A.2, figure A.2.

3.2.2 The Atom-Dimer Scattering Amplitude

The next stage is to derive the dimer-atom scattering amplitude $i\mathcal{A}_3$. The integral equation of this amplitude is shown diagrammatically in figure 3.4. It has been shown previously in section 3.1.2 that for identical bosons the result is independent of the choice of inertial reference frame, therefore the centre-of-mass frame is used where the total momentum of the incoming and outgoing particles is 0: $q_1 = -p_1$ and $q_2 = -p_2$. With total energy ω_T, the equation for the dimer-atom scattering of

identical bosons is formulated as:

$$\begin{aligned}\mathcal{A}_3(q_1,q_2,\omega_T) = &-\frac{\lambda_0^2}{4}\frac{1}{(\omega_T-\omega_{q1}-\omega_{q2})-\frac{(q_1+q_2)^2}{2m}+i\epsilon}-\frac{\gamma_0}{36}\\ &-\frac{1}{2}\int_{-\infty}^{\infty}\frac{d\omega}{2\pi}\int\frac{dk^3}{(2\pi)^3}[(\frac{\lambda_0^2}{4}\frac{1}{(\omega_T-\omega_{q2}-\omega)-\frac{(q_2+k)^2}{2m}+i\epsilon}+\frac{\gamma_0}{36})\\ &\times(\frac{i}{\omega-\frac{k^2}{2m}+i\epsilon}\frac{Z_\Psi}{\frac{m}{a}-m\sqrt{(\frac{k^2}{4}-(\omega_T-\omega)m-i\epsilon)}})am^2\mathcal{A}_3(q_1,k,\omega_T)]\end{aligned}$$

In the treatment of identical bosons,

$$\begin{aligned}\mathcal{A}_3(q_1,q_2,\omega_T) = &-\frac{\lambda_0^2}{4}\frac{1}{(\omega_T-\omega_{q1}-\omega_{q2})-\frac{(q_1+q_2)^2}{2m}+i\epsilon}-\frac{\gamma_0}{36}\\ &-\frac{1}{2}\int_{-\infty}^{\infty}\frac{d\omega}{2\pi}\int\frac{dk^3}{(2\pi)^3}[(\frac{\lambda_0^2}{4}\frac{1}{(\omega_T-\omega_{q2}-\omega)-\frac{(q_2+k)^2}{2m}+i\epsilon}+\frac{\gamma_0}{36})\\ &\times(\frac{i}{\omega-\frac{k^2}{2m}+i\epsilon}\frac{Z_\Psi}{\frac{m}{a}-m\sqrt{(\frac{k^2}{4}-(\omega_T-\omega)m-i\epsilon)}})am^2\mathcal{A}_3(q_1,k,\omega_T)]\end{aligned}$$

Given that the poles of the three-body amplitude are in the upper half complex plane, the only ω-pole of the above integral equation that is in the lower half complex plane is $\omega \to \frac{k^2}{2m} - i\epsilon$. Proceeding in the same manner as for the two-body scattering amplitude in section 3.1.2, let

$$\begin{aligned}I_{\omega,3} = &\int_{-\infty}^{\infty}\frac{d\omega}{2\pi}[(\frac{\lambda_0^2}{4}\frac{1}{(\omega_T-\omega_{q2}-\omega)-\frac{(q_2+k)^2}{2m}+i\epsilon}+\frac{\gamma_0}{36})\\ &\times(\frac{i}{\omega-\frac{k^2}{2m}+i\epsilon}\frac{Z_\Psi}{\frac{m}{a}-m\sqrt{(\frac{k^2}{4}-(\omega_T-\omega)m-i\epsilon)}})am^2\mathcal{A}_3(q_1,k,\omega_T)]\end{aligned}$$

after a change of the variable ω to z, we perform the contour integral of ω through the lower half plane. The real line integral equals the negative of the clockwise contour integral as the contribution of the large radius curve vanishes just as for C. This simplifies the integral as:

$$\begin{aligned}I_{\omega,3} = &-(\frac{\lambda_0^2}{4}\frac{1}{(\omega_T-\omega_{q2}-\frac{k^2}{2m})-\frac{(q_2+k)^2}{2m}+i\epsilon}+\frac{\gamma_0}{36})\\ &\times\frac{-Z_\Psi}{\frac{m}{a}-m\sqrt{(\frac{k^2}{4}-\omega_T m+\frac{k^2}{2}-i\epsilon)}}am^2\mathcal{A}_3(q_1,k,\omega_T)]\end{aligned}$$

We simplify further with the kinematic values $\omega_{q1} = \frac{q_1^2}{2m_2} = \frac{q_1^2}{2m_2}$, $\omega_{q2} = \frac{q_2^2}{2m_2}$:

$$\begin{aligned}\mathcal{A}_3(q_1,q_2,\omega_T) = &-\frac{\lambda_0^2}{4}\frac{1}{\omega_T-\frac{q_1^2}{m}-\frac{q_2^2}{m}-\frac{q_1\cdot q_2}{m}+i\epsilon}-\frac{\gamma_0}{36}\\ &+\frac{1}{2(2\pi)^3}\int dk^3[(\frac{\lambda_0^2}{4}\frac{1}{\omega_T-\frac{q_2^2}{m}-\frac{k^2}{m}-\frac{q_2\cdot k}{m}+i\epsilon}+\frac{\gamma_0}{36})\\ &\times\frac{-Z_\Psi}{\frac{m}{a}-m\sqrt{(\frac{3k^2}{4}-\omega_T m-i\epsilon)}}am^2\mathcal{A}_3(q_1,k,\omega_T)]\end{aligned}$$

The total angular momentum l is set to $l = 0$ and the amplitude projected onto this sector. Let θ be the angle between q_1 and q_2 while φ is the angle between q_1 and k. In the lower energy limit of the ultracold gas regime the scattering amplitude may be projected onto the states with angular momentum number $l = 0$ by averaging over $\cos\theta$ in the tree level diagrams and $\cos\varphi$ in the loop level diagrams:

$$\begin{aligned}
\mathcal{A}_{3,l=0}(q_1,q_2,\omega_T) = &-\int_{-1}^{1} d\cos\theta \frac{\lambda_0^2}{8} \frac{-\frac{m}{q_1 q_2}}{-\frac{\omega_T m}{q_1 q_2} + \frac{(q_1^2+q_2^2)}{q_1 q_2} + \cos\theta - i\epsilon} - \frac{\gamma_0}{36} \\
&+ \frac{1}{2(2\pi)^3} \int dk^3 [\int_{-1}^{1} d\cos\varphi (\frac{\lambda_0^2}{8} \frac{-\frac{m}{q_2 k}}{-\frac{\omega_T m}{q_2 k} + \frac{(q_2^2+k^2)}{q_2 k} + \cos\varphi - i\epsilon} + \frac{\gamma_0}{36}) \\
&\times \frac{-Z_\Psi}{\frac{m}{a} - m\sqrt{(\frac{3k^2}{4} - \omega_T m - i\epsilon)}} am^2 \mathcal{A}_3(q_1,k,\omega_T)] \\
= &\frac{m}{q_1 q_2} \frac{\lambda_0^2}{8} \ln(\frac{-\omega_T m + (q_1^2+q_2^2) + q_1 q_2 - i\epsilon}{-\omega_T m + (q_1^2+q_2^2) - q_1 q_2 - i\epsilon}) - \frac{\gamma_0}{36} \\
&+ \frac{1}{4\pi^2} \int_0^\Lambda dk [k^2 (\frac{m^3 a \lambda_0^2}{8 q_2 k} \ln(\frac{-\omega_T m + (q_2^2+k^2) + q_2 k - i\epsilon}{-\omega_T m + (q_2^2+k^2) - q_2 k - i\epsilon}) - \frac{\gamma_0 a m^2}{36}) \\
&\times \frac{Z_\Psi}{m\sqrt{(\frac{3k^2}{4} - \omega_T m - i\epsilon)} - \frac{m}{a}} \mathcal{A}_3(q_1,k,\omega_T)]
\end{aligned}$$

In order to remove the dependence on λ_0, multiply by Z_Ψ to make the integral equation self-consistent as $Z_\Psi \mathcal{A}_3(q_1,k,\omega_T) \to \mathcal{A}_3(q_1,k,\omega_T)$ and set the dimensionless running parameter $G(\Lambda) \equiv -\frac{\Lambda^2}{m}\frac{\gamma_0}{9\lambda_0^2}$:

$$\begin{aligned}
\mathcal{A}_{3,l=0}(q_1,q_2,\omega_T) = &\frac{16\pi}{ma} \left[\frac{1}{2q_1 q_2} \ln(\frac{-\omega_T m + (q_1^2+q_2^2) + q_1 q_2 - i\epsilon}{-\omega_T m + (q_1^2+q_2^2) - q_1 q_2 - i\epsilon}) + \frac{G(\Lambda)}{\Lambda^2} \right] \\
&+ \frac{16m}{\pi} \int_0^\Lambda dk \left(\frac{1}{8q_2 k} \ln(\frac{-\omega_T m + (q_2^2+k^2) + q_2 k - i\epsilon}{-\omega_T m + (q_2^2+k^2) - q_2 k - i\epsilon}) + \frac{G(\Lambda)}{\Lambda^2} \right) \\
&\times \frac{k^2}{m\sqrt{(\frac{3k^2}{4} - \omega_T m - i\epsilon)} - \frac{m}{a}} \mathcal{A}_{3,l=0}(q_1,k,\omega_T)
\end{aligned} \tag{3.28}$$

The term $G(\Lambda)$ must have a special dependence on Λ for the theory to become renormalisable. The parameter $G(\Lambda)$ is not expected to depend on the two-body scattering length a, but as a dimensionless running constant it must instead be a function of a dimensionless ratio $\frac{\Lambda}{\Lambda_*}$ where Λ_* is the three-body parameter previously introduced as part of the Efimov effect in section 2.3, equation (2.31).

3.2.3 Renormalisation of Three-Body Term $G(\Lambda)$

The integral in equation (3.28) is generally divergent, and so certain considerations must be made for the scattering amplitude $\mathcal{A}_{3,l=0}$ to perform renormalisation $\Lambda \to \frac{1}{l_{\text{vdW}}}$. We must analyse the contributions that the scattering amplitude makes to the integral as the internal momentum k is increased, and see how it is possible to tune the scaling parameter $G(\Lambda)$ to diminish the effect of these contributions on the modulus and phase of $\mathcal{A}_{3,l=0}$.

First reviewing the region $q_2 \to \infty$ with $G(\Lambda)/\Lambda^2 \to 0$, the inhomogeneous term

$$\mathcal{A}_{3,l=0,\text{inh}}(q_1, q_2, \omega_T) = \frac{2\pi}{ma}\left[\frac{1}{q_1 q_2}\ln\left(\frac{-\omega_T m + (q_1^2+q_2^2) + q_1 q_2 - i\epsilon}{-\omega_T m + (q_1^2+q_2^2) - q_1 q_2 - i\epsilon}\right)\right], \tag{3.29}$$

does not have a divergence for $\Lambda \to \infty$ and can be neglected in the investigation of high momentum behavior. Then we set the ansatz $\mathcal{A}_{3,l=0}(q_1, q_2, \omega_T) = A q_1^{s-1}$, supposing that s is imaginary and the modulus of this scattering amplitude is dependent on q_1^{-1}, which will allow the integral to be convergent:

$$q_1^{s-1} = \frac{32m}{8\pi}\int_0^\Lambda dk \left(\frac{1}{2q_2 k}\ln\left(\frac{-\omega_T m + (q_2^2+k^2) + q_2 k - i\epsilon}{-\omega_T m + (q_2^2+k^2) - q_2 k - i\epsilon}\right)\right)\frac{k^2 k^{s-1}}{m\sqrt{\left(\frac{3k^2}{4} - \omega_T m - i\epsilon\right)} - \frac{m}{a}}$$

We can at this point eliminate $-\omega_T m - i\epsilon$ and $\frac{1}{a}$ as they are much smaller than k^2 and k respectively, and change the variable $k = x q_2$

$$q_2^{s-1} = \frac{4}{\pi\sqrt{3}}\frac{1}{q_2}\int_0^\Lambda dx x^{s-1} q_2^s \ln\left(\frac{x^2+x+1}{x^2-x+1}\right)$$

This produces the equation $1 = \frac{4}{\pi\sqrt{3}}\int_0^\Lambda dx x^{s-1}\ln\left(\frac{x^2+x+1}{x^2-x+1}\right)$. It is evaluated as a Mellin transform, by first factorising the x polynomials within the logarithm with roots $x_1 = \frac{1-i\sqrt{3}}{2}$, $x_2 = \frac{1+i\sqrt{3}}{2}$ and using the identity $M[\ln(\frac{x+y}{x-y})] = \pi y^s \tan\frac{\pi s}{2}$:

$$\begin{aligned}\frac{\pi\sqrt{3}}{4} &= \int_0^\Lambda dx x^{s-1}\left[\ln\left(\frac{x+x_1}{x-x_1}\right) + \ln\left(\frac{x+x_2}{x-x_2}\right)\right] \\ &= \pi\frac{(e^{-i\frac{\pi s}{6}} + e^{i\frac{\pi s}{6}})(e^{i\frac{\pi s}{2}} - e^{i\frac{\pi 2}{2}})}{2i\cos\frac{\pi s}{2}}\end{aligned}$$

This gives the transcendental equation

$$\frac{\sqrt{3}s}{8} = \frac{\sin\frac{\pi s}{6}}{\cos\frac{\pi s}{2}}. \tag{3.30}$$

and for two species of bosons with distinct masses m_1, m_2:

$$\frac{\sqrt{1 + \frac{2}{(1+\frac{m_1}{m_2})}}s}{2(1+\frac{m_1}{m_2})} = \frac{\sin\frac{\pi s}{6}}{\cos\frac{\pi s}{2}}. \tag{3.31}$$

The solution $s = \pm i s_0$ must be fully imaginary, and s_0 determines the Efimov spectrum scaling parameter λ described in section 2.5 and the general expression of $\mathcal{A}$ in the high momentum limit:

$$\mathcal{A}_{3,q_2\to\infty} = A_+ q_2^{-1+is_0} + A_- q_2^{-1-is_0} \tag{3.32}$$

We can now study the contribution to $\mathcal{A}_3$ in the momentum region $\frac{1}{a}, q_1, \sqrt{m\omega_T} \ll k \ll \Lambda$ using this new ansatz from equation (3.32). We expect that these contributions affect the phase and amplitude of the log-periodic solution of $\mathcal{A}_3$ in the high-momentum limit, and that compensating for them with $G(\Lambda)$ will lead to a

scale-invariant result for all momenta, which will allow for theory renormalisation using low-energy observables such as the atom-dimer scattering length [21]. The scaling contributions to the amplitude denoted as $\mathcal{A}_3^+$ become:

$$\mathcal{A}_3^+ = \int_{k_0 \gg \frac{1}{a}}^{\Lambda} dk[\frac{1}{k^2} + \frac{G(\Lambda)}{\Lambda^2}] \times (A_+ k^{is_0} + A_- k^{-is_0}) \tag{3.33}$$

The tuning for $G(\Lambda)$ must be motivated by these contributions tending as $\frac{1}{\Lambda^2}$:

$$G(\Lambda) = \frac{\frac{A_+}{1-is_0}\Lambda^{is_0} + \frac{A_-}{1+is_0}\Lambda^{-is_0}}{\frac{A_+}{1+is_0}\Lambda^{is_0} + \frac{A_-}{1-is_0}\Lambda^{-is_0}} \tag{3.34}$$

The coefficients $A_\pm$ can be chosen to depend on the three-body parameter Λ_* so that

$$A_+ = \frac{1}{2}\sqrt{(1+s_0^2)}\Lambda_*^{-is_0}, \qquad A_- = \frac{1}{2}\sqrt{(1+s_0^2)}\Lambda_*^{is_0}.$$

Inserting these into equation (3.34):

$$\begin{aligned} G(\Lambda) &= \frac{\sqrt{\frac{(1+is_0)}{(1-is_0)}}(\frac{\Lambda}{\Lambda_*})^{is_0} + \sqrt{\frac{(1-is_0)}{(1+is_0)}}(\frac{\Lambda}{\Lambda_*})^{-is_0}}{\sqrt{\frac{(1-is_0)}{(1+is_0)}}(\frac{\Lambda}{\Lambda_*})^{is_0} + \sqrt{\frac{(1+is_0)}{(1-is_0)}}(\frac{\Lambda}{\Lambda_*})^{-is_0}} \\ &= \frac{e^{is_0 \ln(\frac{\Lambda}{\Lambda_*}) + i\arctan(s_0)} + e^{-is_0 \ln(\frac{\Lambda}{\Lambda_*}) - i\arctan(s_0)}}{e^{is_0 \ln(\frac{\Lambda}{\Lambda_*}) - i\arctan(s_0)} + e^{-is_0 \ln(\frac{\Lambda}{\Lambda_*}) + i\arctan(s_0)}} \end{aligned}$$

leading to the analytical function of what is called the three-body scaling term:

$$G(\Lambda;\Lambda_*) = \frac{\cos(s_0 \ln(\frac{\Lambda}{\Lambda_*}) + \arctan(s_0))}{\cos(s_0 \ln(\frac{\Lambda}{\Lambda_*}) - \arctan(s_0))}. \tag{3.35}$$

It is demonstrated using numerical testing in section 4.1.1 that this analytical result for $G(\Lambda)$ is an accurate renormalisation group limit cycle for the purposes of determining the atom-dimer scattering amplitude $\mathcal{A}_{3,l=0}$.

3.3 Observables of the Three-Body System

The atom-dimer scattering amplitude provided by equation (3.28) inherits certain properties from the three-body scaling term $G(\Lambda)$ that manifests themselves both as a dependence of the atom-dimer scattering length on the three-body parameter Λ_* and as discrete scaling symmetries of the Efimov spectrum. These effects depend explicitly on the solution for the parameter s_0, which is different for identical bosons and bosons with general mass ratios.

Just as for two-body scattering, the $\mathcal{T}$ matrix element for atom-dimer scattering is found at minimum kinetic energy required for elastic scattering. For $q_2 = -q_1$, the $\mathcal{T}$-matrix element becomes:

$$\mathcal{T}_{q_1,p_1,q_2,p_2} = \mathcal{A}_{3,l=0}(q_1, q_1, \frac{3q_1^2}{4m} - \frac{1}{ma^2}). \tag{3.36}$$

The differential cross-section is in the case of bosons of identical masses:

$$\frac{d\sigma}{d\Omega} = \frac{2m}{3k}\frac{km}{6\pi^2}|\mathcal{A}_{3,l=0}(q_1, q_1, \frac{3q_1^2}{4m} - \frac{1}{ma^2})|^2 = \frac{m^2}{9\pi^2}|\mathcal{A}_{3,l=0}(q_1, q_1, \frac{3q_1^2}{4m} - \frac{1}{ma^2})|^2, \quad (3.37)$$

and similarly to the discussion in section 2.4 for two-body scattering of non-identical particles, the effective range expansion applied to atom-dimer scattering states that for the atom-dimer scattering length a_{AD}, $f_0 = -a_{\mathrm{AD}}$ and

$$\frac{d\sigma}{d\Omega}_{\mathrm{atom,dimer}} = |a_{\mathrm{AD}}|^2,$$

it follows that in the low-energy limit for bosons $q_1 \to 0$ the atom dimer scattering length is given by:

$$a_{\mathrm{AD}} = -\frac{m}{3\pi}\mathcal{A}_{3,l=0}(0, 0, -\frac{1}{ma^2}). \quad (3.38)$$

It is useful to also define the function

$$C(q_1, q_2, \omega_T) = \frac{ma}{8\pi}\frac{\mathcal{A}_{3,l=0}(q_1, q_2, \omega_T)(q_1^2 - q_2^2)}{-\frac{1}{a} + \sqrt{\frac{3q_1^2}{4} - m\omega_T}}, \quad (3.39)$$

which at $q_1 = q_2 = 0$ reduces to $C(0, 0, -\frac{1}{ma^2}) = -a_{\mathrm{AD}}$.
Poles of the scattering amplitude $\mathcal{A}_{3,l=0}$ constitute the spectrum of the three-body bound states known as trimers. For energies ω_T near the threshold energies $-E_3^{(n)}$ of these trimers, the Green's function is factorised into two bound-state functions:

$$\mathcal{A}_{3,l=0}(q_1, q_2, \omega_T) = \frac{\mathcal{B}^{(n)}(q_1)\mathcal{B}^{(n)}(q_2)}{(\omega_T + E_3^{(n)})} \quad (3.40)$$

Setting this into equation (3.28) gives for the case of the identical bosons:

$$\mathcal{B}^{(n)}(q_2) = \frac{4}{\pi}\int_0^\Lambda dk \left(\frac{1}{2q_2k}\ln(\frac{-\omega_T m + (q_2^2 + k^2) + q_2k - i\epsilon}{-\omega_T m + (q_2^2 + k^2) - q_2k - i\epsilon}) + \frac{G(\Lambda)}{\Lambda^2}\right) \quad (3.41)$$
$$\times \frac{k^2}{\sqrt{(\frac{3k^2}{4} - \omega_T m - i\epsilon)} - \frac{1}{a}}\mathcal{B}^{(n)}(k)$$

For the case of two distinct species of bosons with mass ratio $\frac{m_1}{m_2} = \mathrm{r}_m$, the scattering amplitude is modified by other symmetry factors and the mass is replaced with the reduced mass. We only consider the case where the scattering length of the distinct species a_{12} is tuned by Feshbach resonance to be much greater than the scattering length of two identical atoms a_{11} and a_{22}, as this precludes the involvement of corresponding dimer states and simplifies the bound state equation for two m_1 and one m_2 atoms to take the form:

$$\mathcal{B}_{112}^{(n)}(q_2) = \frac{16}{\pi}\int_0^\Lambda dk \left(\frac{1 + \mathrm{r}_m}{32q_2k}\ln(\frac{-2\omega_T m_{\mathrm{r}} + (q_2^2 + k^2) + \frac{2}{(1+\mathrm{r}_m)}q_2k - i\epsilon}{-2\omega_T m_{\mathrm{r}} + (q_2^2 + k^2) - \frac{2}{(1+\mathrm{r}_m)}q_2k - i\epsilon}) + \frac{G(\Lambda)}{\Lambda^2}\right) \quad (3.42)$$
$$\times \frac{k^2}{\sqrt{(\frac{k^2(1+\frac{4}{1+\mathrm{r}_m})}{4} - 2\omega_T m_{\mathrm{r}} - i\epsilon)} - \frac{1}{a_{12}}}\mathcal{B}_{112}^{(n)}(k)$$

4

Results

This chapter presents the results acquired from numerical calculations of the zero-range model values discussed in sections 3.2 and 3.3. Gauss-Legendre quadrature was used to solve the bound state and three-body scattering amplitude equations formulated as Fredholm equations of the second kind.
Confirmation of the renormalization utility of a three-body parameter dependent scaling term $G(\Lambda;\Lambda_*)$ is done with results in section 4.1.1. Section 4.1.2 provides results for the dependence of the atom-dimer scattering length on the proportion $\frac{\Lambda}{\Lambda_*}$ and on the diatomic scattering length.
Section 4.2.1 demonstrates in detail the Efimov effect in systems of identical bosons. The discrete scaling symmetries of the Efimov effect have been satisfied for up to six trimer branches in both the binding energy spectrum at the resonant limit $|a| \to \infty$ and for diatomic scattering lengths characterising the thresholds to the atom-dimer and triatom states with the trimer region. In addition to this, universal scaling curves are represented for the ratios of atom-dimer to diatom scattering lengths, and the ratio of the two shallowest dimers with the dimer binding energy. Section 4.2.2 provides some of the results for the emergence of the Efimov effect in search of a critical value of the mass ratio $\mathrm{r}_m = \frac{m_1}{m_2}$ at which the fermionic system produces a spectrum of trimers that satisfy a discrete scaling symmetry.

4.1 Results for Scattering Amplitudes of Identical Bosons in the Zero-Range Model

The results procured in this section used Gauss-Legendre quadrature procedure outlined in the appendix B.3 to solve the integral equations for $\mathcal{A}_{3,l=0}$ and C numerically. The quadrature procedure for solving $\mathcal{A}_{3,l=0}$ used 15 quadrature points and interpolation, while the procedure for C used 100 quadrature points and no interpolation. The functions and variables are scaled by mass m and scattering length a.

4.1.1 Renormalisation of the Three-Body Scattering Amplitude

Figure 4.1 shows a comparison of the analytical function for $G(\Lambda)$ in equation (3.35) from section 3.2.3 to most effective numerical tests of G, as well as the $\mathcal{A}_{3,l=0}$ identical bosons scattering amplitude graphs evaluated at zero incoming atom momentum $q_2 = 0$ and at total energy $E = -\frac{1}{ma^2}$ for increasing ultraviolet cutoffs. The results are not fully conclusive, as the best fit results do coincide with the analytical $G(\Lambda)$,

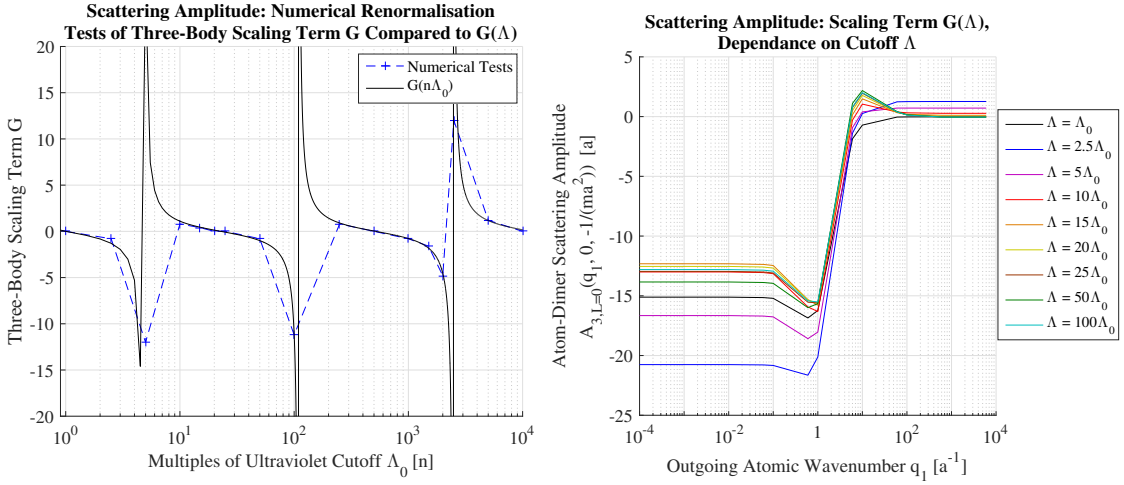

Figure 4.1: Left: Comparison of numerical tests of G to the analytic ansatz $G(\Lambda)$. The result is consistent and shows promise for the validity of the renormalisation provided by inclusion of the three-body parameter $\Lambda_* = 0.9522a^{-1}$ in the theory. $\Lambda_0 = 2.165\Lambda_* : G(\Lambda_0) \approx 0$. Right: scattering amplitudes $\mathcal{A}_{3,L=0}(q_1, 0, -\frac{1}{ma^2})$ for increasing ultraviolet cutoffs indicate a significant changes in the value of the amplitude at $q_1 < \frac{1}{a}$, thereby affecting the atom-dimer scattering length result despite renormalisation of $G(\Lambda)$.

but the numerical procedure determining the scattering amplitude seems to be non-convergent for low values of q_1.
As an alternative a modified scattering amplitude $C(q_1, 0, -\frac{1}{ma^2})$ given by equation (3.39) is evaluated using a non-interpolative method with significantly higher number of quadrature points described in appendix B.3.1, and uses a higher ultraviolet cutoff $\Lambda_0 = 1152\Lambda_* : G(\Lambda_0) \approx 0$. For modified scattering amplitude function $C(q_1, 0, -\frac{1}{ma^2})$ with $G = 0$, the expected log-periodic behavior for high outgoing momenta q_1 are shown in figure 4.2. This confirms the assessment made in section 3.2.3 that the high-momentum form of the scattering amplitude $\mathcal{A}_{3,l=0}$ would asymptotically tend to the form of log-periodic q^{1-is_0}. Using the arguments from section 3.2.3, the effect of including a non-zero G term in C on the amplitude and phase of the function can be seen in figure 4.3.
Using the analytical function of $G(\Lambda)$ given in equation (3.35), the renormalisation of the three-body is demonstrated for large values of the ultraviolet cutoff in the results from figures 4.4 and 4.5. The inclusion of the analytical parameter $G(\Lambda)$ forces the function $C(q_1, 0, -\frac{1}{ma^2})$ evaluated with any ultraviolet cutoff Λ back into the same phase and amplitude as the one evaluated for Λ_0. As the three-body parameter G is the same for the atom-dimer scattering amplitude $\mathcal{A}_{3,l=0}$ as it is for the modified function C, the renormalisation group limit cycle is satisfied, and the low-momentum value of $\mathcal{A}_{3,l=0}$ becomes scale-invariant, confirming that the physical observable atom-dimer scattering length of the theory is renormalised.

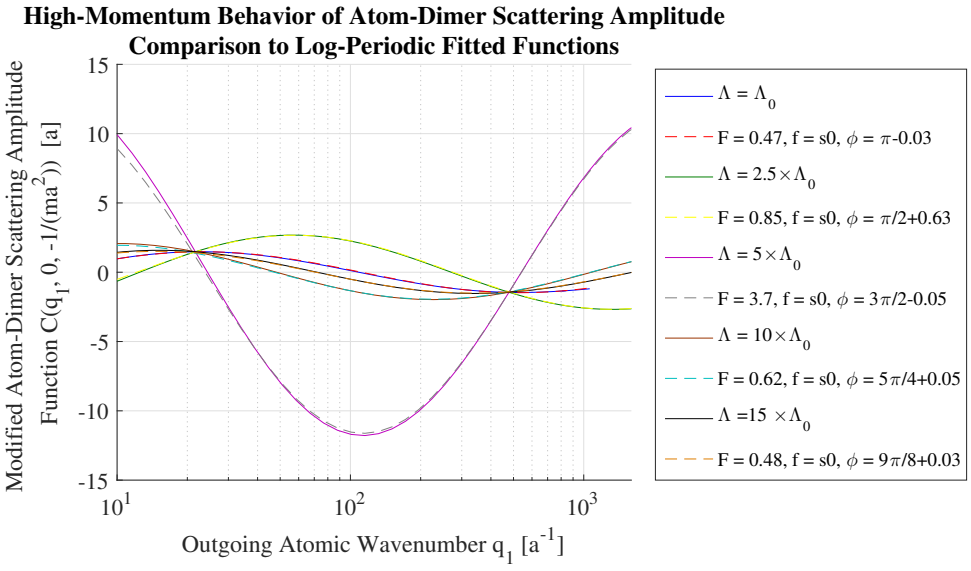

Figure 4.2: Comparison of the $C(q_1, 0, -\frac{1}{ma^2})$ function displayed as solid lines with fitted log-periodic functions $F\cos(f\ln(q_1)+\phi)$. It is demonstrated that for all cutoffs, the frequency f is $s_0 \approx 1.00624$ and that the phase and amplitude of the function are dependent on the cutoff Λ.

4.1.2 Results for the Atom-Dimer Scattering Length

The modified scattering amplitude function $C(q_1, 0, -\frac{1}{ma^2})$ is determined independently by the parameters of diatomic scattering length a and the three-body parameter Λ_* when the ultraviolet cutoff Λ is set at a specific value in terms of the scattering length. This is shown by the results of scattering amplitude graphs in figure 4.6 as a and Λ_* are varied. Additionally it is demonstrated that the atom-dimer scattering length $a_{\mathrm{AD}} = -C(0, 0, -\frac{1}{ma^2})$ depends on the three-body parameter Λ_*.

4.2 Results for Three-Body Bound State Energy in the Zero-Range Model

The results in this section implemented Gauss-Legendre quadrature using 20 quadrature points through the procedure outlined in appendix B.2.

4.2.1 Results for Bound State Energy of Identical Bosons

The Efimov effect and its universal discrete scaling symmetries have been reproduced in 6 trimer branches using the bound state equation (3.41) in section 3.3 for identical bosons as seen in figure 4.7. The values of the binding energies increase in depth by a factor of approximately $\lambda^2 = 22.7^2$ in the resonant limit while the diatom scattering lengths associated with trimer-three atom threshold $a = a_+$ and the trimer-dimer threshold $a = a_-$ decrease by the factor λ as shown in figure 4.8. Because the solution parameter for identical bosons $s_0 \approx 1.00624$, this is consistent with the

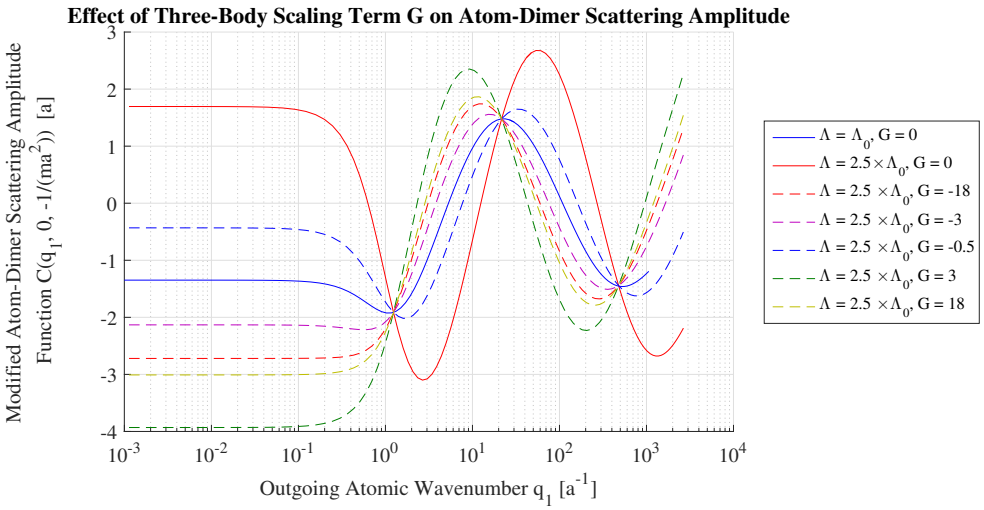

Figure 4.3: Comparison of modified scattering amplitude function $C(q_1, 0, -\frac{1}{ma^2})$ visualises the effect of the three-body scaling term. Solid lines are with $G = 0$ evaluated at ultraviolet cutoffs $\Lambda = \Lambda_0$ and $\Lambda = 2.5\Lambda_0$, dashed lines are with non-zero values of G evaluated at ultraviolet cutoff $\Lambda = 2.5\Lambda_0$. The phase and amplitude of the dashed lines are shifted, while the frequency remains unchanged. This confirms that there may exist $G(\Lambda)$ such that leaves the scattering amplitude invariant for all momenta $q_1 < \Lambda$.

relation for the discrete scaling parameter $\lambda = e^{\frac{\pi}{s_0}}$ described in section 2.5, and the Efimov trimer spectrum of equation (2.30) is developed with $n^* := 0$. Additionally, comparison to atom-dimer scattering length as well as the ratios of first and second trimer binding energies to the dimer binding energy E_D shown in figure 4.9 are consistent with the universal scaling curves found in literature [18].
For quantum degenerate gases, we view these universal results of the zero-range Model in the three-body sector as predictions for the reactions of optically trapped Bose-Einstein gases and condensates in the ultracold regime to the tuning of the diatomic scattering length using Feshbach resonance. The universal model predicts, besides the scaling symmetries viewed in figures 4.7 and 4.8, the existance of infinitely many trimer branches at ever shallower energies [18]. These trimer branches indicate directly a strongly interacting quantum degenerate gas is formed that allows for three-atom bound states at ranges of large scattering lengths $[-\infty, a_{(-)}]$ and $[a_{(+)}, \infty]$ in the ultracold regime. For our results, trimer branches (1) and (2) remain within the ultra-cold regime and the threshold points $a_{(-)}, a_{(+)}$ where these trimer branches intersect with the x-axis and the dimer line E_{D} signify values of a at which the bound trimer state is in resonance with a three-atom state and an atom-dimer state respectively.
When such resonances occur in trapped Bose-Einstein gases, the binding energy of the trimer can be released into the kinetic energy of the three atoms at the x-axis threshold, which occurs for certain negative scattering lengths a, or into the kinetic energy of the dimer-atom pair at the E_{D} threshold for specific positive scattering lengths a [11]. These energies may exceed the confinement properties of the optical trap, leading to escaping gas atoms at these resonance points, called loss effects.

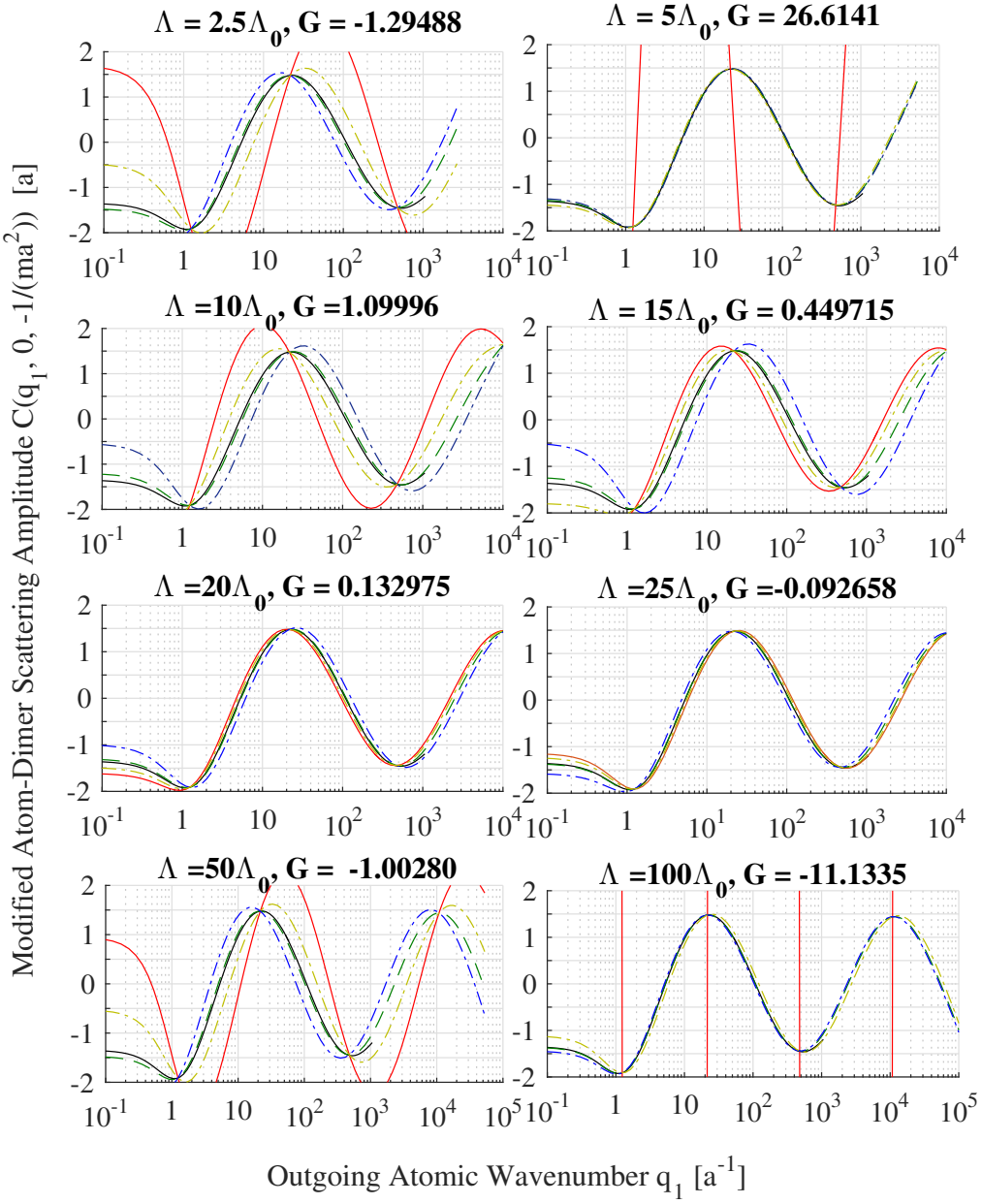

Figure 4.4: Renormalisation demonstrated with modified scattering amplitude $C(q_1, 0, -\frac{1}{ma^2})$. The solid black line in each graph indicates the function $C(q_1, 0, -\frac{1}{ma^2})$ evaluated with ultraviolet cutoff Λ_0 and $G(\Lambda_0) = 0$. Solid red line is for a variable cutoff Λ and $G = 0$, dashed green line is for analytical solution $G(\Lambda)$, blue and yellow dash-dotted lines are $2 \times G(\Lambda)$ and $\frac{2}{5} \times G(\Lambda)$ respectively. Evidently the numerical solution provides the renormalisation required to shift the phase and amplitude of C back to the Λ_0 line.

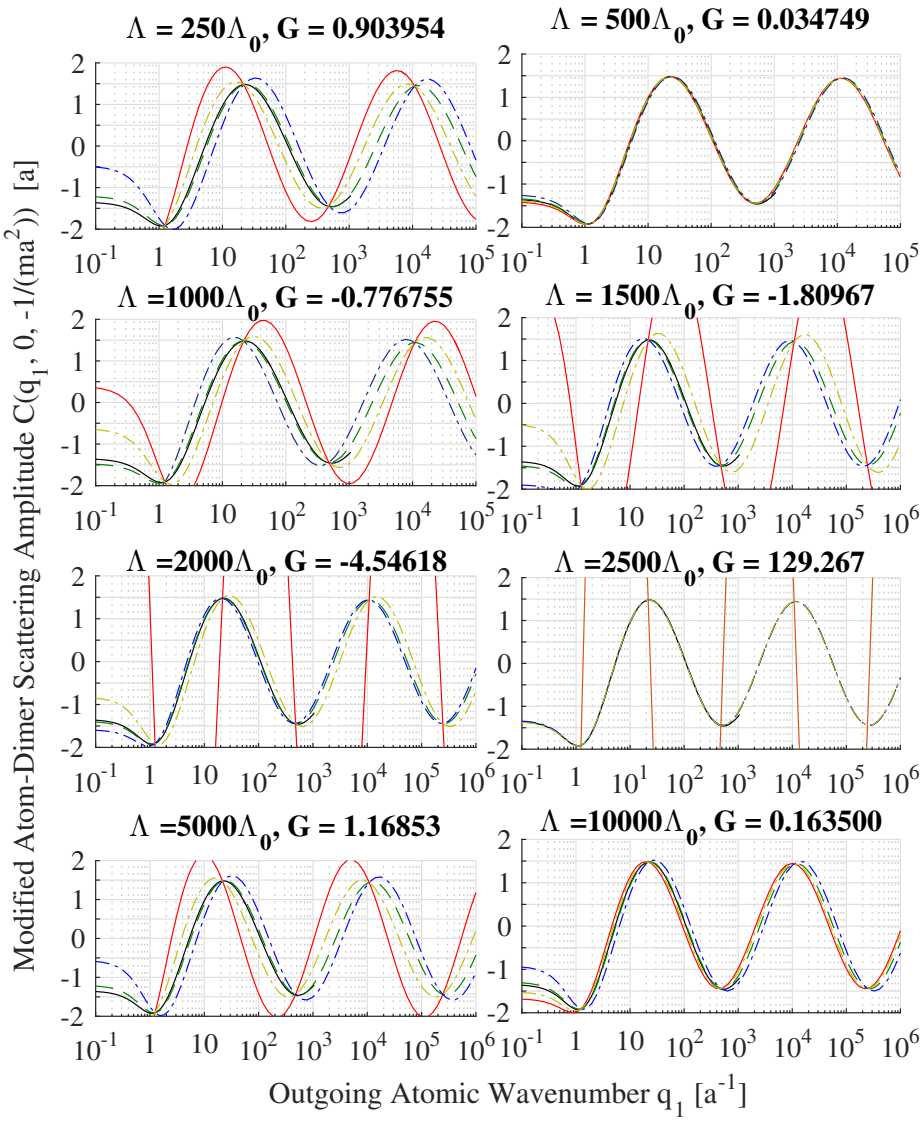

Figure 4.5: Continuation of figure 4.4 for even greater ultraviolet cutoffs. Although the renormalisation still provides scale-invariance, it should be noted that the zero-range model is not expected to provide accurate predictions for the high-momentum region and it is meaningless to study ultraviolet cutoffs that exceed the natural energy scale of the system by several orders of magnitude.

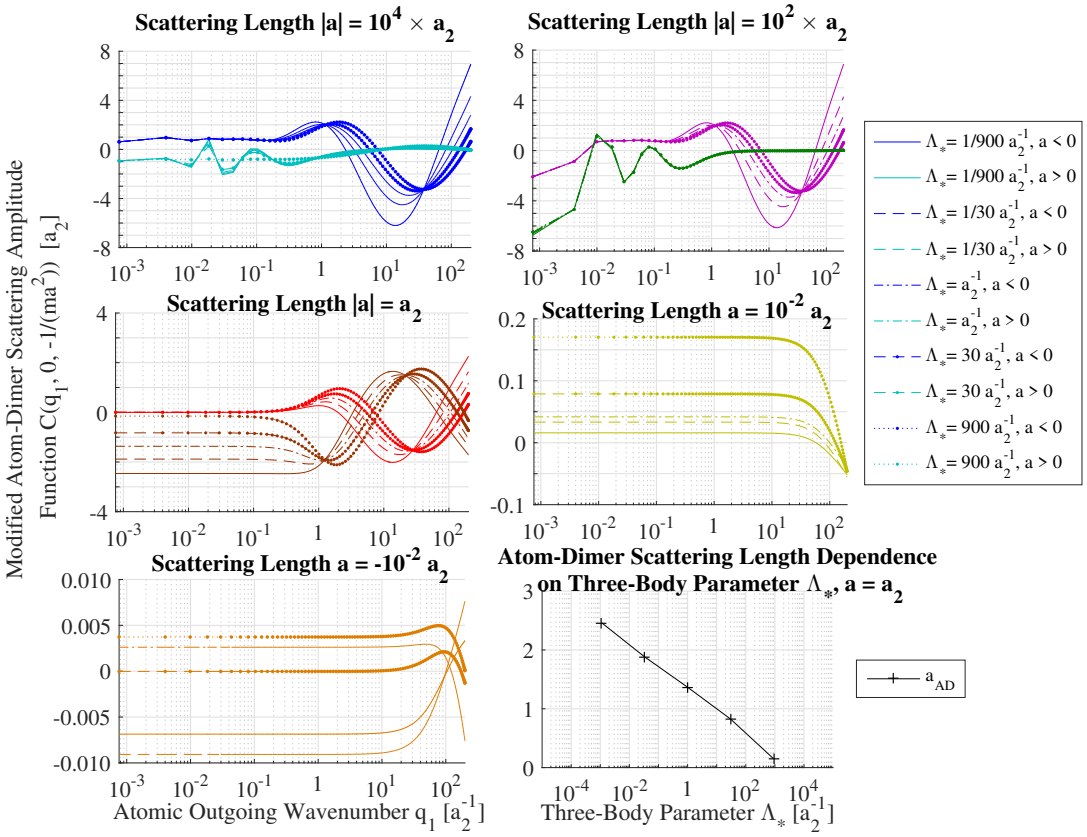

Figure 4.6: Graphs 1-5 show modified atom-dimer scattering amplitudes for a wide set of diatomic scattering lengths a and a variety of three-body parameters Λ_*. Blue, purple, red and orange lines are for negative scattering lengths $a < 0$ while teal, green, brown and yellow lines are for positive scattering lengths $a > 0$. Graph 6 shows the locally linear dependence of the atom-dimer scattering length on the order of magnitude of the three-body parameter. Ultraviolet cutoff $\Lambda = 200a_2^{-1}$ for all measurements.

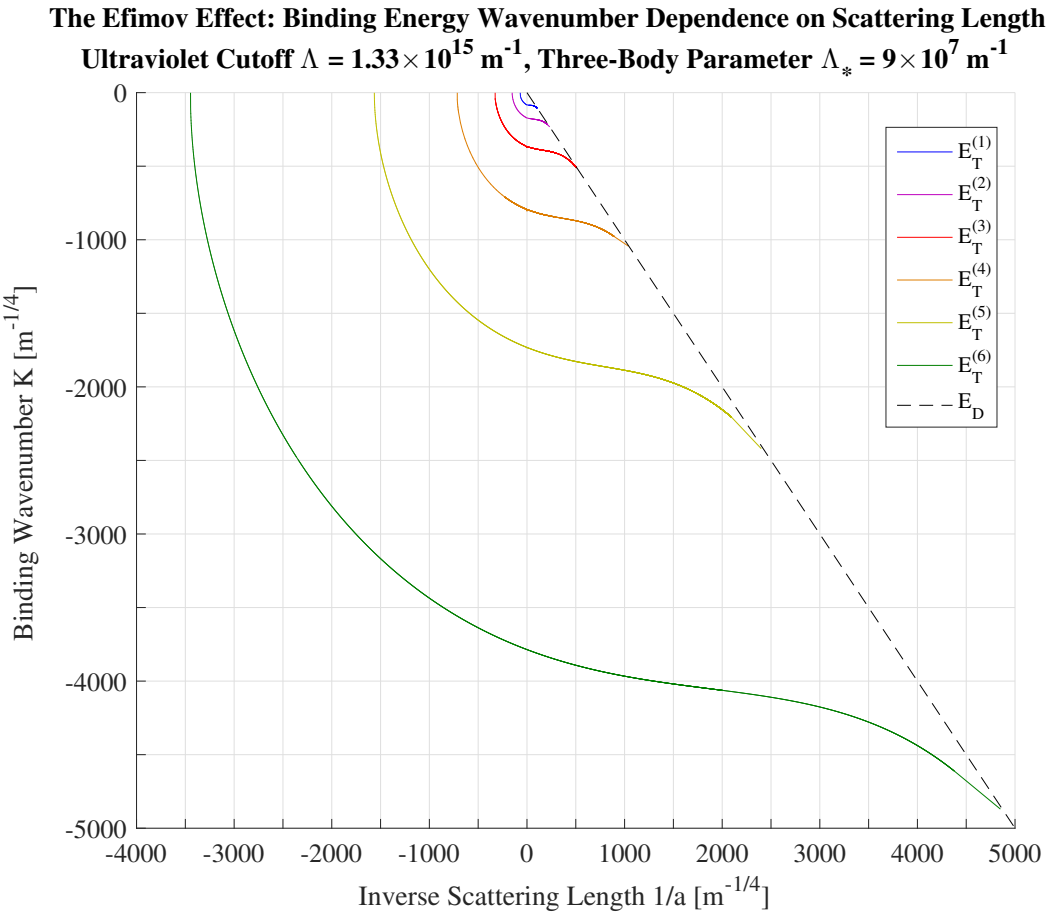

Figure 4.7: The six branches of trimers constituent of three identical bosons. The binding wavenumber and inverse scattering length are scaled by a transformation $x_i \to \frac{x_i}{(\sqrt{x_1^2+x_2^2})^{\frac{3}{4}}}$ in order to fit all 6 trimer branches. The straight line in the fourth quadrant indicates the threshold to atom-dimer energy favorable systems, and the x axis for negative scattering lengths $a < 0$ is the threshold for three-atom energy favorable systems. Between these thresholds lies the domain of the bosonic trimer. The energy E_{T} of a trimer branch can be computed as $\frac{\hbar^2 K^2}{m}$ where m is the mass of a given atomic species.

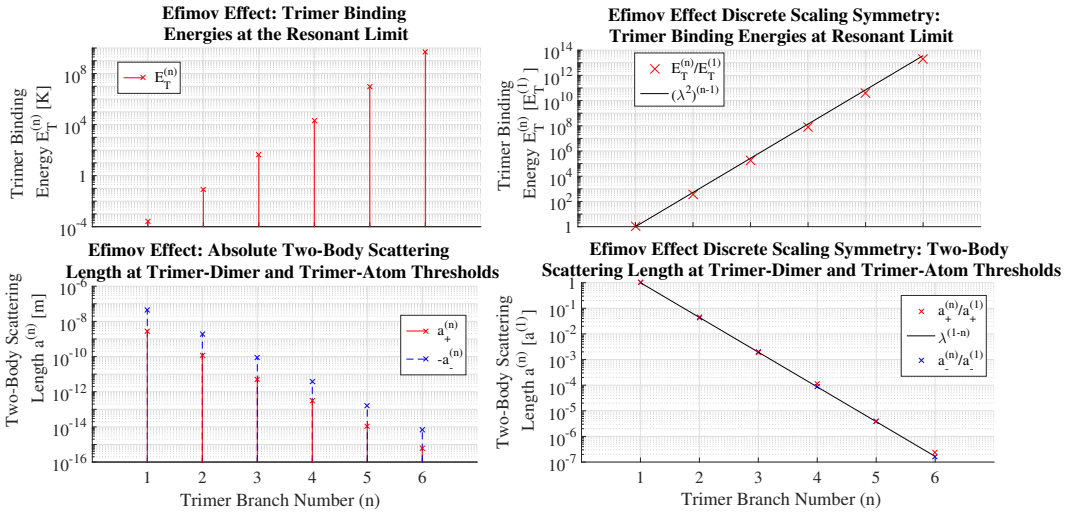

Figure 4.8: Discrete scaling symmetries and absolute values of trimer binding energies at the resonant limit and threshold scattering lengths. The absolute energy was computed using the mass of He^4, and the scale of the temperatures of the deeper trimers far exceeds the energy scales of the ultracold regime necessary for the s-wave approximation to be valid. The threshold scattering lengths also decrease into the infinitesimal, with the lowest reaching a length lower than 10^{-15} m - the scale of the charge radius of a proton. It's likely that these deeper trimer branches are not naturally realisable.

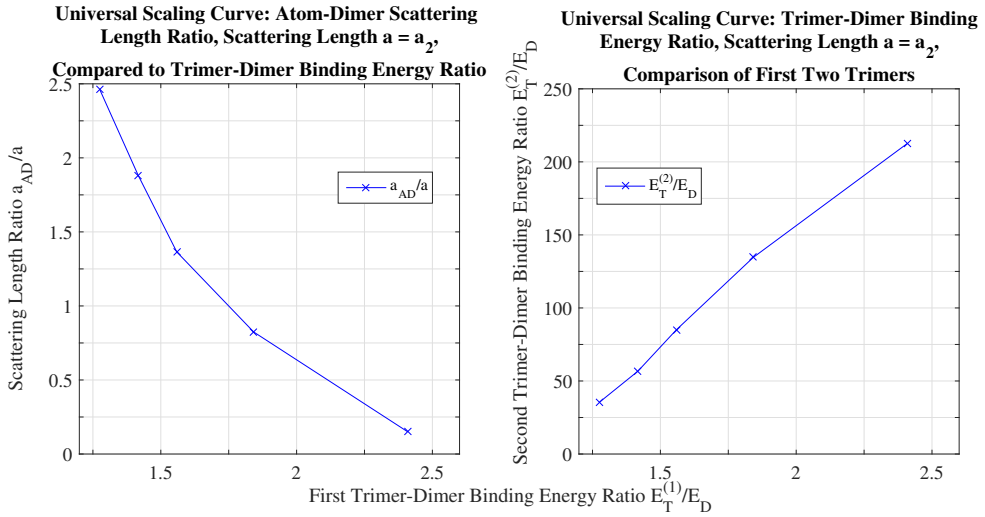

Figure 4.9: Universal scaling curves of the ratios $\frac{a_{\mathrm{AD}}}{a_2}$, $\frac{E_{\mathrm{T}}^{(1)}}{E_{\mathrm{D}}}$ and $\frac{E_{\mathrm{T}}^{(2)}}{E_{\mathrm{D}}}$ for various Λ_*. Scaling violations are apparent for these values as the three-body parameter Λ_* is altered.

These scattering lengths have a discrete scaling symmetry determined by the Efimov effect, and of express importance is that deeper trimers require the tuning of ever lower scattering lengths to observe these resonances and their loss effects - if the scattering length is tuned to be shorter than the natural length scale of the studied atomic species, its van der Waals length, the results and predictions of the zero-range model lose their validity. Although the universality of the zero-range model does also predict resonances for very high values of $|a|$, the binding energy levels for shallower trimers become ever lower and therefore harder to detect in the laboratory. Yet the research of the ultracold regime Bose-Einstein condensate continues, and perhaps in the future more of these bound states will be found, allowing for a better understanding of the strong interactions in bosonic quantum degenerate gases.

4.2.2 Results for Bound State Energy of Distinct Bosons

The Efimov effect has been reproduced for mixtures of bosons with distinguishable masses. The mass ratios tested were $\frac{m_1}{m_2} = \{0.9, 2, 5, 10\}$ using equation (3.42), the bound state equation for two atoms of mass m_1 and one atom of mass m_2, and the scattering length of mixed atoms tuned greater than all other diatomic scattering lengths using Feshbach resonance. The results of the emergent Efimov spectrum trimer branches are shown in figure 4.10.
It is demonstrated that increasing the mass ratio for $m_1 > m_2$ will produce more tightly spaced trimer branches. For masses $m_2 > m_1$, however the discrete scaling factor λ grows and the deeper trimer branches quickly fall outside the scope of the ultracold regime in order of magnitude. Figure 4.11 shows the plot of the solutions s_0 of the transcendental equation (3.31) as a function of the mass ratio $\mathrm{r}_m = \frac{m_1}{m_2}$ and the results for the discrete scaling symmetry factors λ of these mixed boson gas systems, confirming that the Efimov effect is satisfied.

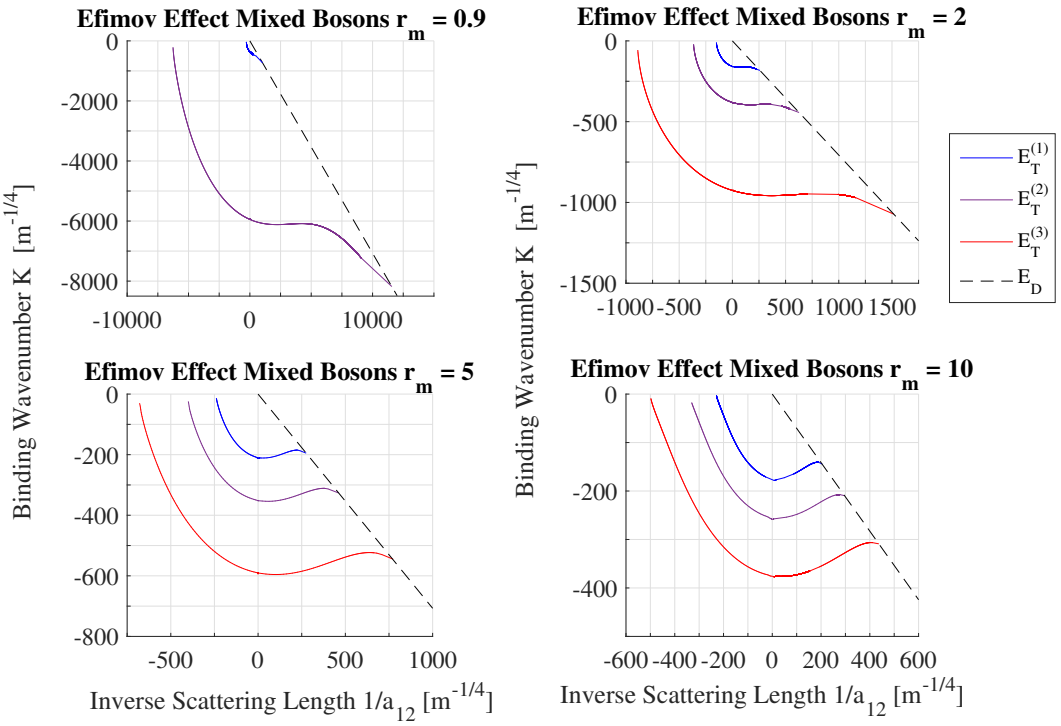

Figure 4.10: The binding energy branches of trimers constitutent of mixed bosons, two with mass m_1 and one with mass m_2, mass ratio $\mathrm{r}_m = \frac{m_1}{m_2}$ and mixed diatomic scattering length a_{12} tuned greater than self-pair scattering lengths a_{11}, a_{22}. In order to fit the branches, the inverse scattering length and the binding wavenumber are scaled $x_i \to \frac{x_i}{(\sqrt{x_1^2+x_2^2})^{\frac{3}{4}}}$. The dashed straight line indicates the dimer binding energy $E_\mathrm{D} = -\frac{1}{m_\mathrm{r} a_{12}^2}$. The three-body parameter is set for all graphs as $\Lambda_* = 9 \times 10^7$ m^{-1}.

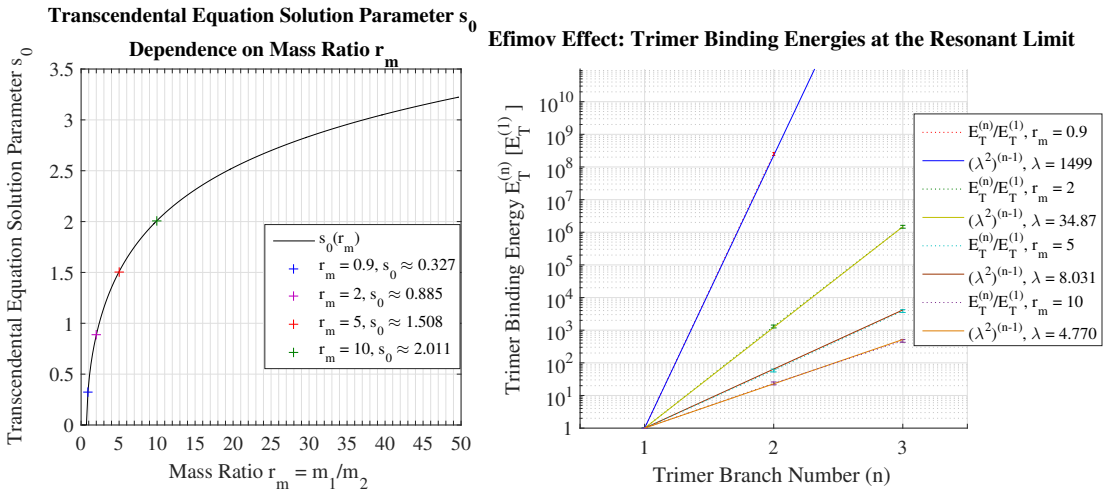

Figure 4.11: Left: plot of the transcendental equation solution parameter s_0 dependency on the mass ratio $\mathbf{r}_m$. The values of s_0 cease to be real at $\mathrm{r}_m \approx 0.74$ and the Efimov effect does not occur for mass ratios at or below this point. Right: the discrete scaling symmetries for the four trimer sets. The ratios of trimer binding energies at the resonant limit correspond well to the scaling factors $\lambda^2 = e^{\frac{2\pi}{s_0}}$ predicted by the Efimov effect.

5
Conclusion

From the work outlined in this thesis, we have applied the zero-range model developed in the context of nuclear physics to procure a set of predictions for the three-body physics of Bose-Einstein gases in the ultracold temperature regime.
It has been successfully demonstrated for bosons that the model is applicable to the three-body sector using a parameter three-body Λ_* with which a renormalisation group transformation is performed so that the atom-dimer scattering amplitude and the atom-dimer scattering length become scale-invariant. It has also been demonstrated that the result for the atom-dimer scattering length will depend on this three-body parameter.
The Efimov effect has been reproduced for bosons and the discrete scaling symmetries inherent to the Efimov effect have been verified for the trimer branches' threshold scattering lengths toward the three-atom state and the atom-dimer state, as well as for the binding energy at the resonant limit. A universal scaling curve has been reproduced that demonstrates the scaling violations of the atom-dimer scattering length and the trimer binding energies at the resonant limit. The Efimov effect has also been confirmed to occur for gases composed of mixtures of bosons, and that the mass ratio directly impacts the energy level spacing of the bound three-body state spectrum.
In conclusion, this thesis has demonstrated the applicability of the effective field theory known as the zero-range model, with the results parametrised by the spin-statistic, masses, and scattering lengths of the gas atoms with inclusion of an experimentally discernible three-body parameter Λ_* for the renormalisation of the three-body problem, to describe the three-body physics of quantum degenerate gases in the ultracold regime.

Bibliography

[1] V. Efimov, "Energy levels of three resonantly interacting particles," *Nuclear Physics A*, vol. **210**, no. 1, (1973).

[2] H.-W. Hammer and L. Platter, "Efimov States in Nuclear and Particle Physics," *Annual Review of Nuclear and Particle Science*, vol. **60**, no. 1, (2010).

[3] K. G. Wilson, "Renormalization Group and Strong Interactions," *Phys. Rev. D*, vol. **3**, 8 (1971).

[4] J. Thomas and M. Gehm, "*Optically Trapped Fermi Gases*," *American Scientist - AMER SCI*, vol. **92**, (2004).

[5] M. Köhl, H. Moritz, T. Stöferle, K. Günter, and T. Esslinger, "Fermionic atoms in a Three Dimensional Optical Lattice: Observing Fermi Surfaces, Dynamics, and Interactions," *Phys. Rev. Lett.*, vol. **94**, (2005).

[6] W. Ketterle, D. Durfee, and D. Stamper-Kurn, "Making, probing and understanding Bose-Einstein condensates," (1999). arXiv preprint cond-mat/: 9904034.

[7] G. Salomon, L. Fouché, S. Lepoutre, A. Aspect, and T. Bourdel, "All-optical cooling of K^{39} to Bose-Einstein condensation," *Physical Review A*, vol. **90**, (2014).

[8] F. Pereira Dos Santos, J. Léonard, J. Wang, *et al.*, "Bose-Einstein Condensation of Metastable Helium," *Phys. Rev. Lett.*, vol. **86**, (2001).

[9] S. Baier, D. Petter, J. H. Becher, *et al.*, "Realization of a Strongly Interacting Fermi Gas of Dipolar Atoms," *Phys. Rev. Lett.*, vol. **121**, (2018).

[10] I. Bloch, J. Dalibard, and W. Zwerger, "Many-Body Physics with Ultracold Gases," *Reviews of Modern Physics*, vol. **80**, pp. 885–964, (2008).

[11] T. Kraemer, M. Mark, P. Waldburger, *et al.*, "Evidence for Efimov quantum states in an ultracold gas of caesium atoms," *Nature*, vol. **440**, no. 7082, (2006).

[12] M. H. Anderson, J. R. Ensher, M. R. Matthews, C. E. Wieman, and E. A. Cornell, "Observation of Bose-Einstein Condensation in a Dilute Atomic Vapor," *Science*, vol. **269**, (1995).

[13] D. B. Spalding, "The Molecular Theory of Gases and Liquids," *The Journal of the Royal Aeronautical Society*, vol. **59**, (1955).

[14] E. Braaten, M. Kusunoki, and D. Zhang, "Scattering models for ultracold atoms," *Annals of Physics*, vol. **323**, (2008).

[15] J. Dalibard, "Collisional dynamics of ultracold atomic gases," (2002).

[16] J. J. Sakurai, *Modern quantum mechanics; rev. ed.* Reading, MA: Addison-Wesley, (1994).

[17] L. D. Landau and L. M. Lifshitz, *Quantum Mechanics Non-Relativistic Theory, Third Edition: Volume 3*. Butterworth-Heinemann, (1981), ISBN: 0750635398.

[18] E. Braaten and H.-W. Hammer, "Universality in few-body systems with large scattering length," *Physics Reports*, vol. **428**, (2006).

[19] P. F. Bedaque, H.-W. Hammer, and U. van Kolck, "Renormalization of the Three-Body System with Short-Range Interactions," *Physical Review Letters*, vol. **82**, no. 3, (1999).

[20] S. Weinberg, *The Quantum Theory of Fields*. Cambridge University Press, (1995), vol. **1**.

[21] P. Bedaque, H.-W. Hammer, and U. van Kolck, "The Three-Boson System with Short-Range Interactions," *Nuclear Physics A*, vol. **646**, no. 4, (1999).

A

Appendix: Feynman Rules

A.1 Zero-range model, two-body sector

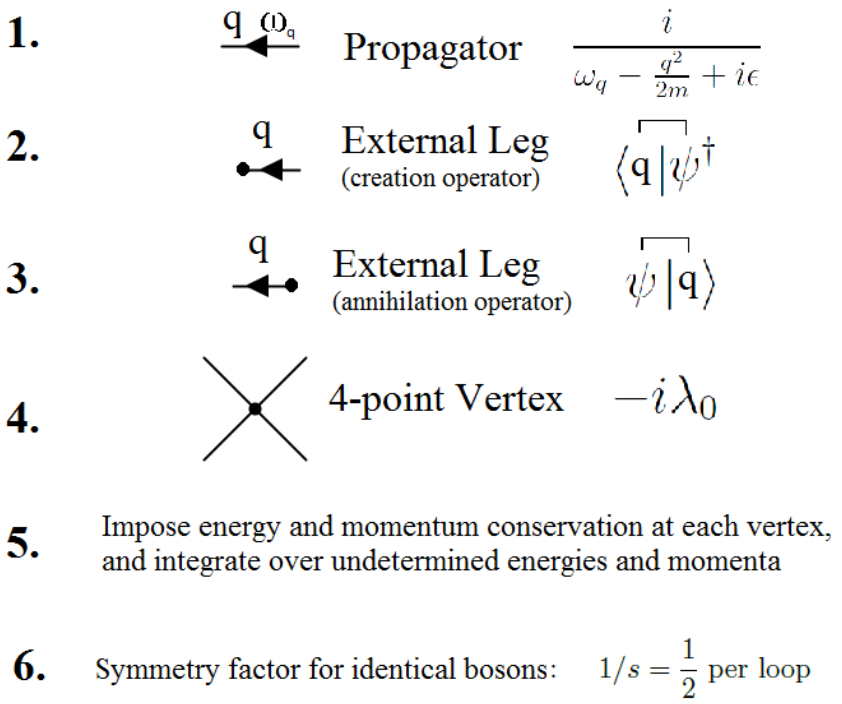

Figure A.1: The Feynman rules for the two-body sector zero range model includes the retarded causal propagator, the external legs for creation and annihilation operators, and the four point vertex. The energy and momenta are conserved on each vertex. For identical bosons a symmetry factor $\frac{1}{2}$ is implemented for every loop. Undetermined momenta and energies are integrated over for each loop.

A.2 Zero-range model, three-body sector

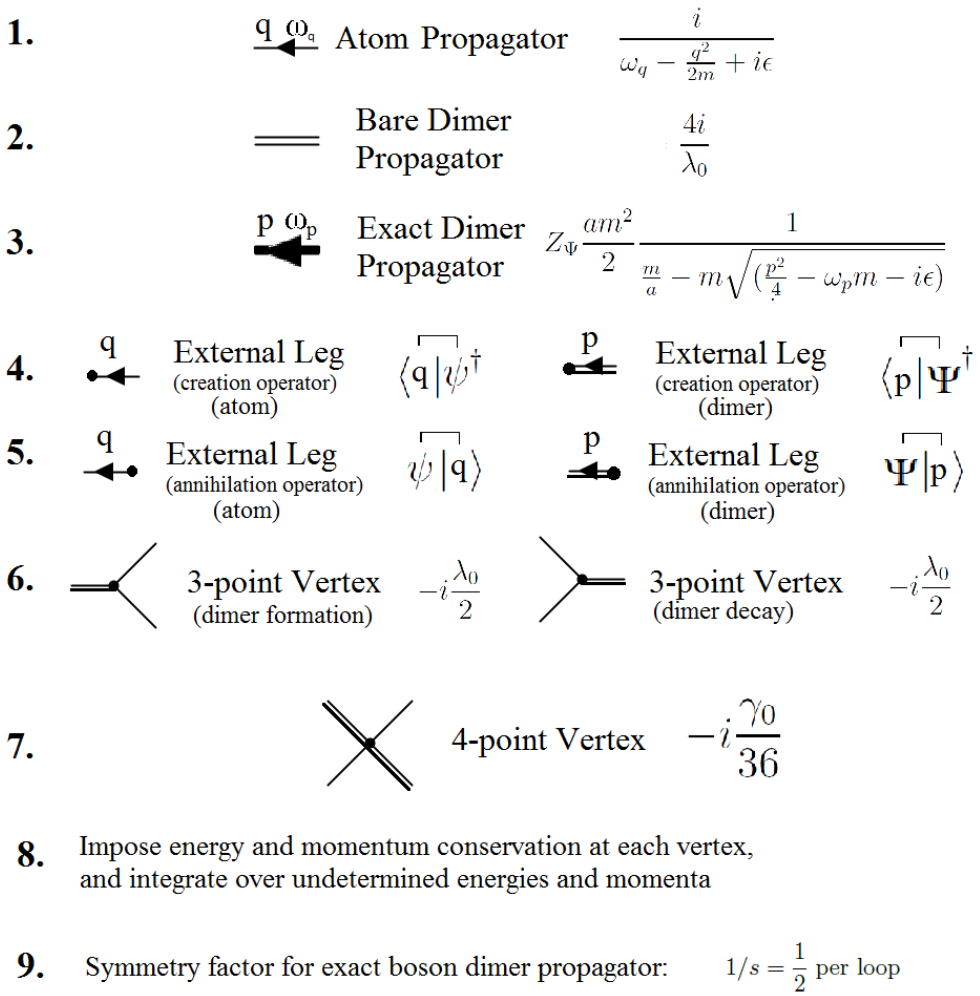

Figure A.2: The Feynman rules for the three-body sector zero range model includes the retarded causal atom propagator, the bare and exact dimer propagators, the external legs for creation and annihilation operators, the three point dimer-atom vertices and the four point dimer-atom vertex. The energy and momenta are conserved on each vertex. For the computation of the exact dimer propagator with identical bosons a symmetry factor $\frac{1}{2}$ is implemented for every loop. Undetermined momenta and energies are integrated over for each loop.

B

Appendix: Numerical Methods

B.1 Gauss-Legendre Quadrature

The bound state equation for three-body interactions is a homogeneous Fredholm integral equation:

$$\begin{aligned}\mathcal{B}^{(n)}(q_2,\omega_T) &= \frac{4}{\pi}\int_0^\Lambda dk\left(\frac{1}{2q_2k}\ln\left(\frac{-\hbar\omega_T m+\hbar^2(q_2^2+k^2)+\hbar^2q_2k-i\epsilon}{-\hbar\omega_T m+\hbar^2(q_2^2+k^2)-\hbar^2q_2k-i\epsilon}\right)+\frac{G(\Lambda)}{\Lambda^2}\right)\\ &\quad\times\frac{k^2}{\frac{1}{\hbar}\sqrt{\left(\frac{3\hbar^2k^2}{4}-\hbar\omega_T m-i\epsilon\right)}-\frac{1}{a}}\mathcal{B}^{(n)}(k,\omega_T)\\ &= \int_0^\Lambda dkK(k,q_2,\omega_T)\mathcal{B}^{(n)}(k,\omega_T)\end{aligned}$$

Where the scale-dependent three body running constant $G(\Lambda)$ is for a choice Λ_*:

$$G(\Lambda)=\frac{\cos\left(s_0\ln\left(\frac{\Lambda}{\Lambda_*}\right)+\arctan\left(s_0\right)\right)}{\cos\left(s_0\ln\left(\frac{\Lambda}{\Lambda_*}\right)-\arctan\left(s_0\right)\right)} \tag{B.1}$$

It is expected that there exist energies $-E_3^{(n)}=\hbar\omega^{(n)}$ such that $B^{(n)}(q,\omega^{(n)})$ are solutions of the bound state equation. These energies are also poles of the three-body scattering amplitude function $\mathcal{A}_{l=0}$. To find these energies it is necessary to set a condition for when the bound state equation is satisfied by the energy.
Numerically, it is possible to implement Gauss-Legendre quadrature to approximate the integral as a sum of the function values $K(k,q_2)\mathcal{B}^{(n)}(k)$ evaluated at specific points, multiplied by corresponding weights:

$$\mathcal{B}^{(n)}(q_{2i},\omega_T)=\sum_{j=1}^{N}w_jK(k_j,q_{2i},\omega_T)\mathcal{B}^{(n)}(k_j,\omega_T) \tag{B.2}$$

The points q_{2i} and k_j are abcissae - the roots of the Legendre polynomials $P^{(N)}(x_j)=0$ while the weights are computed as:

$$w_j=\frac{2}{(1-x_j)^2|\partial_xP^{(N)}(x)|^2_{x_j}} \tag{B.3}$$

However, these choices of weights and abcissae are only valid for integrals taken on the interval $[-1,1]$. The strength of the Gauss-Legendre quadrature method is that

for any Legendre polynomial of degree $n+1$, $P_{n+1}(x)$ is orthogonal to all polynomials $Q(x)$ of degree n or lower:

$$\int_{-1}^{1} P_{n+1}(x)Q(x)dx = 0. \tag{B.4}$$

If I let the integrated function be factorised as $f(x) = Q(x)P_{n+1}(x)+r(x)$, $f(x)$ can be a polynomial up to degree $2n+1$ while the property in equation (B.4) holds for $Q(x)$ and $P_{n+1}(x)$. Therefore the integral for such an $f(x)$ polynomial up to degree $2n+1$ on $[-1,1]$ is:

$$\int_{-1}^{1} f(x)dx = \int_{-1}^{1} Q(x)P_{n+1}(x)dx + \int_{-1}^{1} r(x)dx \tag{B.5}$$

The first term is zero, meaning to integrate $f(x)$ exactly it is sufficient to integrate the remainder $r(x)$. The remainder has a degree of at most n, else it would have leading terms divisible by $P_{n+1}(x)$ and therefore part of $Q(x)$. Using n quadrature points the exact integral of $r(x)$ is always found:

$$\int_{-1}^{1} r(x_i)dx = \sum_{i=1}^{n} w_i r(x_i), \tag{B.6}$$

and using the abcissae x_i such that $P_{n+1}(x_i) = 0$, $r(x_i) + Q(x_i)P_{n+1}(x_i) = r(x_i) = f(x_i)$. Therefore for any $f(x)$ that behaves like an $2n+1$ polynomial, the use of Gauss-Legendre quadrature returns an exact integral $\int_{-1}^{1} f(x)dx = \sum_{i=1}^{n} w_i f(x_i)$.
To evaluate the solution numerically, it is first necessary to transform the variables into a dimensionless form by casting them in units of two-body scattering length $|a|$:

$$\hat{k} = |a|k \qquad \hat{q}_2 = |a|q_2$$
$$\hat{\omega}_T = |a|^2\omega_T \qquad \hat{\Lambda} = |a|\Lambda$$

Then the calculation becomes:

$$\begin{aligned}
\mathcal{B}^{(n)}(q_2,\omega_T) = \frac{4}{\pi}\int_0^{\Lambda} dk \left(\frac{1}{2q_2k}\ln\left(\frac{-\hbar\omega_T m + \hbar^2(q_2^2+k^2) + \hbar^2 q_2 k - i\epsilon}{-\hbar\omega_T m + \hbar^2(q_2^2+k^2) - \hbar^2 q_2 k - i\epsilon}\right) + \frac{G(\Lambda)}{\Lambda^2}\right) \\
\times \frac{k^2}{\frac{1}{\hbar}\sqrt{\left(\frac{3\hbar^2k^2}{4} - \hbar\omega_T m - i\epsilon\right)} - \frac{1}{a}}\mathcal{B}^{(n)}(k,\omega_T) \\
\mathcal{B}^{(n)}(\hat{q}_2,\hat{\omega}_T) = \frac{4}{\pi}\int_0^{\hat{\Lambda}} \frac{d\hat{k}}{|a|} \left(\frac{|a|^2}{2\hat{q}_2\hat{k}}\ln\left(\frac{-\hbar\hat{\omega}_T m + \hbar^2(\hat{q}_2^2+\hat{k}^2) + \hbar^2 \hat{q}_2 \hat{k} - i\epsilon}{-\hbar\hat{\omega}_T m + \hbar^2(\hat{q}_2^2+\hat{k}^2) - \hbar^2 \hat{q}_2 \hat{k} - i\epsilon}\right) + \frac{|a|^2 G(\hat{\Lambda}/|a|)}{\hat{\Lambda}^2}\right) \\
\times \frac{\hat{k}^2 \frac{1}{|a|^2}}{\frac{1}{\hbar|a|}\sqrt{\left(\frac{3\hbar^2\hat{k}^2}{4} - \hbar\hat{\omega}_T m - i\epsilon\right)} - \frac{1}{a}}\mathcal{B}^{(n)}(\hat{k},\hat{\omega}_T) \\
\mathcal{B}^{(n)}(\hat{q}_2,\hat{\omega}_T) = \frac{4}{\pi}\int_0^{\hat{\Lambda}} d\hat{k} \left(\frac{1}{2\hat{q}_2\hat{k}}\ln\left(\frac{-\hbar\hat{\omega}_T m + \hbar^2(\hat{q}_2^2+\hat{k}^2) + \hbar^2 \hat{q}_2 \hat{k} - i\epsilon}{-\hbar\hat{\omega}_T m + \hbar^2(\hat{q}_2^2+\hat{k}^2) - \hbar^2 \hat{q}_2 \hat{k} - i\epsilon}\right) + \frac{G(\hat{\Lambda}/|a|)}{\hat{\Lambda}^2}\right) \\
\times \frac{\hat{k}^2}{\frac{1}{\hbar}\sqrt{\left(\frac{3\hbar^2\hat{k}^2}{4} - \hbar\hat{\omega}_T m - i\epsilon\right)} - \mathrm{sign}(a)}\mathcal{B}^{(n)}(\hat{k},\hat{\omega}_T)
\end{aligned}$$

An important feature of this transformation is that the explicit dependence on the scattering length of the solution has been codified into the sign of the scattering length: sign(a) and on the adjustment of the interval - given any cutoff Λ, the interval of integration now also depends on $|a|$. Once the solutions corresponding to $\hat{\omega}_T$ are found the measure of energy measured in Kelvin can be recovered by $E^{(n)} = \frac{\hbar}{k_B|a|^2}\hat{\omega}_T^{(n)}$. The goal is to discover how these energies depend on the scattering length. It is understood the frequency and momenta have distances measured in $|a|$. Because of the log-periodic behaviour of the kernel K, the quadrature points should be evaluated on a logarithmic grid. For this reason it is first best to perform the change of variables $k' = \log(k+1)$, $\frac{dk}{dk'}dk' = e^{k'}dk'$ and shift the interval from $[0,\Lambda]$ to $[0,\ln(\Lambda+1)]$, before finding the Gauss Legendre weights and abcissae for $[0,\ln(\Lambda+1)]$. The same transformation should be applied to q_2 in order to evaluate the left hand side and right hand side on the same quadrature points.

$$k = e^{k'} - 1$$

$$\int_0^{\Lambda} dk K(k,q_2,\omega_T)\mathcal{B}^{(n)}(k,\omega_T) = \int_0^{\ln(\Lambda+1)} e^{k'}dk' K(e^{k'}-1,e^{q_2'}-1,\omega_T)\mathcal{B}^{(n)}(e^{k'}-1,\omega_T)$$

$$\mathcal{B}^{(n)}(e^{q_2'}-1,\omega_T) = \frac{4}{\pi}\int_0^{\ln(\Lambda+1)} \left(\frac{\ln\left(\frac{-\omega_T\frac{m}{\hbar}+e^{2k'}+e^{2q_2'}+e^{k'+q_2'}-3e^{k'}-3e^{q_2'}+3-i\epsilon}{-\omega_T\frac{m}{\hbar}+e^{2k'}+e^{2q_2'}-e^{k'+q_2'}-e^{k'}-e^{q_2'}+1-i\epsilon}\right)}{2e^{k'+q_2'}-e^{k'}-e^{q_2'}+1} + \frac{G(\Lambda/|a|)}{\Lambda^2} \right)$$
$$\times \frac{(e^{2k'}-2e^{k'}+1)}{\sqrt{e^{k'}(\frac{3(e^{2k'}-2e^{k'}+1)dk}{4} - \omega_T\frac{m}{\hbar} - i\epsilon)} - \mathrm{sign}(a)}\mathcal{B}^{(n)}(e^{k'}-1,\omega_T)$$

Finally we replace the parameter $\omega_T\frac{m}{\hbar}$ with the square of the wavenumber $K_E = \mathrm{sign}(\omega_T)\sqrt{|\omega_T|\frac{m}{\hbar}}$. All variables of the equation are now dimensionless. With the kernel thus newly defined, the solution for $\mathcal{B}''^{(n)}(q_2',K_E) = \mathcal{B}^{(n)}(e^{q_2'}-1,K_E)$ can be expressed as the integral on $[-1,1]$:

$$k' = \frac{\ln(\Lambda+1)}{2}k'' + \frac{\ln(\Lambda+1)}{2}$$
$$\mathcal{B}''^{(n)}(q_2',K_E) = \int_{-1}^{1}\frac{\ln(\Lambda+1)}{2}dk'' K(\frac{\ln(\Lambda+1)}{2}k'' + \frac{\ln(\Lambda+1)}{2}, q_2', K_E)$$
$$\times \mathcal{B}''^{(n)}(\frac{\ln(\Lambda+1)}{2}k'' + \frac{\ln(\Lambda+1)}{2}, K_E)$$

The weights are therefore multiplied by the Jacobian factor $\frac{dk'}{dk''} = \frac{\ln(\Lambda+1)}{2}$ and the abcissae are scaled and shifted by $\frac{\ln(\Lambda+1)}{2}$. Using these as points $q_{2i}, k_j = \frac{\ln(\Lambda+1)}{2}k_j'' + \frac{\ln(\Lambda+1)}{2}$ in the discretization of the integral makes makes a linear system of N equations (B.2).

$$\mathcal{B}''^{(n)}(k_i,K_E) - \sum_{j=1}^{N} w_j K(k_j,q_{2i},K_E)\mathcal{B}''^{(n)}(k_j,K_E) = 0$$
$$(\delta_{i,j} - \sum_{j=1}^{N} w_j K(k_j,k_i,K_E))\mathcal{B}''^{(n)}(k_j,K_E) = 0$$
$$(\mathtt{id}_N - M(K_E))\mathcal{B}''^{(n)}(k_j,K_E) = 0$$

Therefore for those K_E where $\mathtt{det}(\mathtt{id}_N - M(K_E)) = 0$, Fredholm equation is satisfied. The associated energy indicates the trimer energy which in units of Kelvin depends on a^2 as well as the solutions being distinctly different depending on the sign of a. An anolagous procedure is performed for the bound state equation associated with fermions of distinct masses.
Mathematica uses the GaussianQuadratureWeights method to find the abcissae and weights for the interval $[0, \ln(\Lambda|a|+1)]$ where Λ is the van-der-Waals length of helium, and the method Det to find the determinant. The dependence on a as a variable in the term $\mathrm{sign}(a)$ and the adjustment of $\hat{\Lambda}$ that determines the integral bounds $[0, \ln(\hat{\Lambda}+1)] = [0, \ln(\Lambda|a|+1)]$ has been implemented. 20 quadrature points were used for the integration of the bound state equation.

B.2 Methodology for Trimer Binding Energies

Currently a bisection method is used to find the zero of a function, is used on the determinant $\mathtt{det}(\mathtt{id}_N - M(K_E))$. The method requires two initial guesses of where to search and the zeroes of the determinant are orders of magnitude apart, so it is best to find at least one set of zeroes graphically to be used as guesses. The bisection method can be bracketted for every guess so that it searches for a guess $K_{E,g}$ on the interval $[b_1 K_{E,g}, b_2 K_{E,g}]$ where $b_2 > b_1 > 0$.
When provided the estimated point for $K_{E,g}$, at the scattering length equal to the bare scattering length of helium, the dependence on a of the trimer energy can be found by lowering or raising the value of a^{-1} while iteratively using the found zeroes as guesses for the next value of a^{-1} after some step Δa^{-1}. The values b_1 and b_2 must be adjusted to satisfy two conditions - the interval must be sufficiently large that after the step δa^{-1} the zeroes of the determinant are found on that interval, and sufficiently small that the interval does not encompass multiple branches, in which case it will not find the trimer branch it was initially set to plot.

B.3 Methodology for Scattering Amplitudes

For the scattering amplitude Green's function in the 0 total angular momentum sector, the coordinate conversion is accomplished also first with conversion to measurement in units of scattering length $\frac{\mathcal{A}_{3,l=0}}{|a|} = \mathcal{A}'_{3,l=0}$:

$$\begin{aligned}\mathcal{A}'_{3,l=0}(q_1,q_2,\omega_T) = \frac{\mathrm{sign}(a)16\pi}{m}\left[\frac{1}{2q_1q_2}\ln\left(\frac{-\omega_T\frac{m}{\hbar}+q_1^2+q_2^2+q_1q_2-i\epsilon}{-\omega_T\frac{m}{\hbar}+q_1^2+q_2^2-q_1q_2-i\epsilon}\right)+\frac{G(\Lambda/|a|)}{\Lambda^2}\right]\\ +\frac{4}{\pi}\int_0^\Lambda dk\left(\frac{1}{2q_2k}\ln\left(\frac{-\omega_T\frac{m}{\hbar}+q_2^2+k^2+q_2k-i\epsilon}{-\omega_T\frac{m}{\hbar}+q_2^2+k^2-q_2k-i\epsilon}\right)+\frac{G(\Lambda/|a|)}{\Lambda^2}\right)\\ \times\frac{k^2}{\sqrt{\left(\frac{3k^2}{4}-\omega_T\frac{m}{\hbar}-i\epsilon\right)}-\mathrm{sign}(a)}\mathcal{A}'_{3,l=0}(q_1,k,\omega_T)\end{aligned}$$

then with conversion to logarithmic grid $k = e^{k'} - 1$, $q_{1,2} = e^{q'_{1,2}} - 1$. Technically q_1 does not need to be transformed in this way as it is not part of the quadrature but

it helps to keep the functions consistent:

$$\mathcal{A}'_{3,l=0}(q_1,q_2,\omega_T)=\frac{\text{sign}(a)16\pi}{m}\left[\frac{\ln\left(\frac{-\omega_T\frac{m}{\hbar}+e^{2q'_1}+e^{2q'_2}+e^{q'_1+q'_2}-3e^{q'_1}-3e^{q'_2}+3-i\epsilon}{-\omega_T\frac{m}{\hbar}+e^{2q'_1}+e^{2q'_2}-e^{q'_1+q'_2}-e^{q'_1}-e^{q'_2}+1-i\epsilon}\right)}{2e^{q'_1+q'_2}-e^{q'_1}-e^{q'_2}+1}+\frac{G(\Lambda/|a|)}{\Lambda^2}\right] \tag{B.7}$$

$$+\frac{4}{\pi}\int_0^{\ln(\Lambda+1)}\left(\frac{\ln\left(\frac{-\omega_T\frac{m}{\hbar}+e^{2k'}+e^{2q'_2}+e^{k'+q'_2}-3e^{k'}-3e^{q'_2}+3-i\epsilon}{-\omega_T\frac{m}{\hbar}+e^{2k'}+e^{2q'_2}-e^{k'+q'_2}-e^{k'}-e^{q'_2}+1-i\epsilon}\right)}{2e^{k'+q'_2}-e^{k'}-e^{q'_2}+1}+\frac{G(\Lambda/|a|)}{\Lambda^2}\right) \tag{B.8}$$

$$\times\frac{e^{k'}(e^{2k'}-2e^{k'}+1)dk}{\sqrt{\left(\frac{3(e^{2k'}-2e^{k'}+1)}{4}-\omega_T\frac{m}{\hbar}-i\epsilon\right)}-\text{sign}(a)}\mathcal{A}'_{3,l=0}(e^{q'_1}-1,e^{k'}-1,\omega_T) \tag{B.9}$$

The inhomogeneous part is here

$$h(e^{q'_1}-1,e^{q'_2}-1,\omega_T)=\frac{\text{sign}(a)16\pi}{m}\left[\frac{\ln\left(\frac{-\omega_T\frac{m}{\hbar}+e^{2q'_1}+e^{2q'_2}+e^{q'_1+q'_2}-3e^{q'_1}-3e^{q'_2}+3-i\epsilon}{-\omega_T\frac{m}{\hbar}+e^{2q'_1}+e^{2q'_2}-e^{q'_1+q'_2}-e^{q'_1}-e^{q'_2}+1-i\epsilon}\right)}{2e^{q'_1+q'_2}-e^{q'_1}-e^{q'_2}+1}+\frac{G(\Lambda/|a|)}{\Lambda^2}\right] \tag{B.10}$$

With $k'=\frac{\ln(\Lambda+1)}{2}k''+\frac{\ln(\Lambda+1)}{2}$, and replacing the parameter $\omega_T\frac{m}{\hbar}$ with the square of the wavenumber $K_E=\text{sign}(\omega_T)\sqrt{|\omega_T|\frac{m}{\hbar}}$, the same quadrature points $q_{2i},k_j=\frac{\ln(\Lambda+1)}{2}k''_j+\frac{\ln(\Lambda+1)}{2}$ and the same kernel as for $\mathcal{B}^{(n)}$, with $\mathcal{A}''(q'_1,q'_2,K_E)=\mathcal{A}''(e^{q'_1}-1,e^{q'_2}-1,K_E)$ and $h'(q'_1,q'_2,K_E)=h(e^{q'_1}-1,e^{q'_2}-1,K_E)$, the integral is discretized and Gauss Legendre quadrature performed to develop a system of N linear equations:

$$\mathcal{A}''_{3,l=0}(q'_1,q_{2i},K_E)-\sum_{j=1}^{N}w_jK(k_j,q_{2i},K_E)\mathcal{A}''_{3,l=0}(q'_1,k_i,K_E)=h'(q'_1,q_{2i})$$

$$(\delta_{i,j}-\sum_{j=1}^{N}w_jK(k_j,k_i,K_E))\mathcal{A}''_{3,l=0}(q'_1,k_i,K_E)=h'(q'_1,q_{2i})$$

$$(\mathtt{id}_N-M(K_E))\mathcal{A}''_{3,l=0}(q'_1,k_i,K_E)=h'(q'_1,q_{2i})$$

The method in Mathematica LinearSolve can then be used to find the solution vector $\mathcal{A}'_{3,l=0}(q'_1,k_i,K_E)$ that satisfies the system of equations. 15 quadrature points were used to solve the atom-dimer scattering amplitude Lipmann-Schwinger equation. Using Nyströms interpolation formula, for a general value of q'_2:

$$\mathcal{A}''_{3,l=0}(q'_1,q'_2,K_E)=h'(q'_1,q'_2)+\sum_{j=1}^{N}w_jK(k_j,q'_2,K_E)\mathcal{A}''_{3,l=0}(q'_1,k_j,K_E) \tag{B.11}$$

Once this interpolation is found, the function $\mathcal{A}'_{3,l=0}(q_1,q_2,K_E)$ can be returned by reversing the coordinate change $q'_1,q'_2=\ln(q_1+1),\ln(q_2+1)$. As this amplitude is

scaled by mass, when determining the atom-dimer scattering length it is sufficient to multiply the amplitude by the mass reduction coefficient rather than the mass as implied by equation (3.38).

B.3.1 Methodology for Three-Body Renormalisation

Because the above procedure was found to be inadequate for the confirmation of the renormalisation group limit cycle due to a lack of consistent, scale-invariant results in the low-energy limit, the modified amplitude $C(q_1, 0, K_E)$ function was studied instead:

$$\begin{aligned} C(q_1, 0, -1) &= \frac{1}{8\pi}\mathcal{A}'_{3,l=0}(q_1, 0, -1)\frac{q_1^2}{-\text{sign}(a) + \sqrt{\frac{3q_1^2}{4} + 1}} \\ &= \frac{1 + \sqrt{\frac{3q_1^2}{4} + 1}}{6\pi}\mathcal{A}'_{3,l=0}(q_1, 0, -1) \end{aligned}$$

while the kernel remains the same, the heterogenous term is multiplied accordingly by this factor $\text{sign}(a)\frac{1+\sqrt{\frac{3q_1^2}{4}+1}}{6\pi}$. Furthermore, instead of using Nyströms interpolation formula, the corresponding Fredholm equation was evaluated using LinearSolve on 100 quadrature points spanning the appropriate range of momenta. In the kinematic limit $q_1 \to 0$, the value of $C(q_1, 0, -1)$ tends towards

$$\frac{1}{3\pi}\mathcal{A}'_{3,l=0}(0, 0, -1) = \frac{m}{3\pi}\mathcal{A}_{3,l=0}(0, 0, -\frac{1}{ma^2}) \tag{B.12}$$

which is as follows from equation (3.38) the negative of the atom-dimer scattering length a_{AD}. Scale-invariant values of $C(q_1, q_2, K_E)$ in this low-energy kinematic limit $q_1, q_2 \to 0, K_E \to -1$, ensures renormalisation of the atom-dimer scattering amplitude.

DEPARTMENT OF PHYSICS
CHALMERS UNIVERSITY OF TECHNOLOGY
Gothenburg, Sweden
www.chalmers.se

CHALMERS
UNIVERSITY OF TECHNOLOGY